The locus coeruleus broadcasts prediction errors across the cortex to promote sensorimotor plasticity

Rebecca Jordan[1,3,4] & Georg B. Keller[1,2]

[1]*Friedrich Miescher Institute for Biomedical Research, Basel, Switzerland.*
[2]*Faculty of Sciences, University of Basel, Basel, Switzerland.*
[3]*Current address: Simons Initiative for the Developing Brain, University of Edinburgh, 1 George Square, EH8 9JZ, Edinburgh, United Kingdom.*
[4]*Correspondence to:* rjordan3@ed.ac.uk

ABSTRACT

Prediction errors are differences between expected and actual sensory input and are thought to be key computational signals that drive learning related plasticity. One way that prediction errors could drive learning is by activating neuromodulatory systems to gate plasticity. The catecholaminergic locus coeruleus (LC) is a major neuromodulatory system involved in neuronal plasticity in the cortex. Using two-photon calcium imaging in mice exploring a virtual environment, we found that the activity of LC axons in the cortex correlated with the magnitude of unsigned visuomotor prediction errors. LC response profiles were similar in both motor and visual cortical areas, indicating that LC axons broadcast prediction errors throughout the dorsal cortex. While imaging calcium activity in layer 2/3 of the primary visual cortex, we found that optogenetic stimulation of LC axons facilitated learning of a stimulus-specific suppression of visual responses during locomotion. This plasticity – induced by minutes of LC stimulation – recapitulated the effect of visuomotor learning on a scale that is normally observed during visuomotor development across days. We conclude that prediction errors drive LC activity, and that LC activity facilitates sensorimotor plasticity in the cortex, consistent with a role in modulating learning rates.

**** Dear reader, please note this manuscript is formatted in a standard submission format, and all statistical information is in Table S1. ****

INTRODUCTION

Through experience with the world, brains learn to predict the sensory feedback generated by movement. For instance, learning the precise relationship between motor commands and the resulting visual

feedback is the basis for both feedback control of movements as well as distinguishing self-generated from externally generated sensory feedback. One way that the brain may learn to do this is via predictive processing (Keller and Mrsic-Flogel, 2018; Rao and Ballard, 1999). In a sensorimotor version of this framework, the brain learns an internal model which transforms motor activity into a prediction of the sensory consequences. The framework postulates that specific neurons are responsible for computing discrepancies – known as prediction errors – between the prediction and the actual sensory inputs received. The neocortex has been shown to compute signals consistent with sensorimotor prediction errors (Eliades and Wang, 2008; Keller and Mrsic-Flogel, 2018; Schneider et al., 2018). In the primary visual cortex (V1), excitatory neurons in layer 2/3 compute mismatches between visual flow speed and locomotion speed (Attinger et al., 2017; Jordan and Keller, 2020; Keller et al., 2012; Zmarz and Keller, 2016). Such sensorimotor prediction error responses in the cortex depend on ongoing and developmental experience with sensorimotor coupling (Attinger et al., 2017; Schneider et al., 2018; Vasilevskaya et al., 2022; Widmer et al., 2022), and therefore the computation underlying them is actively learned. In predictive processing, one main function of prediction errors is to drive corrective plasticity in the internal model that generates predictions (Keller and Mrsic-Flogel, 2018).

During the first sensorimotor experience in life, prediction errors should strongly drive learning of an internal model of the world, while later in life, prediction errors should update internal models primarily when overall prediction errors are abundant (for instance, in novel or volatile situations). One way to implement such a developmental or contextual shift in the amount of plasticity induced by a particular prediction error would be a gating signal. The characteristics of a gating signal are that it is activated by prediction errors and that it permits increases in plasticity. In addition, because it is not driving plasticity, but simply gating it, it can be low dimensional (i.e., the same for all neurons). Prime candidates for a gating signal are neuromodulatory systems. Dopaminergic neurons in the midbrain signal reward prediction errors (Kim et al., 2020; Schultz, 2016) and action prediction errors (Greenstreet et al., 2022), which are thought to gate plasticity in downstream targets to support learning of stimulus-reward associations and goal directed behavior (Cox and Witten, 2019; Flagel et al., 2011; Reynolds et al., 2001; Steinberg et al., 2013). Indeed, the catecholamines – dopamine and noradrenaline – regulate and gate plasticity in the cortex (Choi et al., 2005; He et al., 2015; Seol et al., 2007). However, the midbrain dopaminergic system projects only sparsely to most of the sensory neocortex of the mouse, including V1 (Nomura et al., 2014), where visuomotor predictions are thought to be learned (Attinger et al., 2017; Widmer et al., 2022). Instead, the major catecholaminergic input to the cortex is the locus coeruleus (LC). LC activity has

61 primarily been investigated in the context of classical stimulus presentations and reinforcement tasks.
62 Such studies have shown that the LC responds to many different events, including unexpected task
63 outcomes (Bouret and Sara, 2004; Breton-Provencher et al., 2022), novelty (Takeuchi et al., 2016; Vankov
64 et al., 1995), and unexpected sensory stimuli in general (Aston-Jones and Bloom, 1981; Deitcher et al.,
65 2019; Foote et al., 1980; Hervé-Minvielle and Sara, 1995). In zebrafish, noradrenergic neurons increase
66 their activity during the prolonged visuomotor mismatches of failed swim attempts to drive 'giving up'
67 behavior (Mu et al., 2019). We hypothesized that if the mouse LC is activated during similar visuomotor
68 mismatches, this could represent visuomotor prediction error signaling that would function to gate
69 prediction error driven plasticity in output circuits like the cortex.

70 To test fundamental aspects of this idea, we imaged calcium activity in LC axons in the cortex during
71 visuomotor mismatches, and optogenetically manipulated LC activity levels during visuomotor experience
72 to probe for experience dependent changes in cortical activity. We found that LC axons in both sensory
73 and motor cortical regions respond to unsigned visuomotor prediction errors, i.e., unpredicted visual
74 motion or unpredicted visual halts during locomotion. We then combined optogenetic LC axon stimulation
75 with two-photon calcium imaging of layer 2/3 neurons in V1, to show that the LC greatly facilitates a form
76 of plasticity consistent with predictive visuomotor learning: learned suppression of nasotemporal visual
77 flow responses during forward locomotion. These results support the idea that a key function of the LC is
78 to facilitate prediction error driven cortical plasticity.

79 **RESULTS**

80 We first assessed whether locus coeruleus (LC) axons convey sensorimotor prediction errors to the cortex.
81 To record LC axonal activity, we expressed axon-targeted, Cre-dependent GCaMP6s in noradrenergic
82 neurons of the LC via stereotactic viral vector injections in 13 NET-Cre mice (NET = norepinephrine
83 transporter) (Wagatsuma et al., 2018). We confirmed that these injections labelled only cells in the LC,
84 and that GCaMP6s positive cells were also immunoreactive for tyrosine hydroxylase, a marker for
85 catecholaminergic neurons (**Figure S1A**). For two-photon imaging, we implanted a 4 mm imaging window
86 either over the right V1 and surrounding cortical regions (posterior cortex, 9 mice), or over the right
87 primary and secondary motor cortices (anterior cortex, 4 mice). Prior to imaging, mice were habituated
88 to a virtual reality (VR) system consisting of a virtual tunnel, with walls patterned with vertical sinusoidal
89 gratings (**Figure 1A**). In the closed loop condition, locomotion was coupled to visual movement of the

90 tunnel, and in open loop conditions, the walls moved independent of mouse locomotion. After
91 habituation to head-fixation, we began imaging across up to five non-overlapping fields of view (FoV) in
92 each imaging window, yielding a total of 31 posterior cortex FoVs and 9 anterior cortex FoVs. Axonal
93 fluorescence showed strong correlations with pupil diameter (**Figure S1B**) typical for LC axons (Reimer et
94 al., 2016), rapid responses to air puffs (**Figure S1C**) as previously reported (Breton-Provencher et al., 2022;
95 Deitcher et al., 2019), and increases in fluorescence at locomotion onset that decayed during the
96 locomotion bout (**Figure S2**) consistent with earlier work (Reimer et al., 2016). We found that within a
97 FoV, individual axon segments exhibited highly correlated activity (**Figures 1B and S1D-F**). Given that the
98 algorithms that identify axons (i.e., determine whether two axon segments belong to the same axon) rely
99 on temporal correlations of activity (Leinweber et al., 2017; Mukamel et al., 2009), axon segmentation is
100 difficult in these data. Thus, to prevent oversampling of the data, we pooled data from all axon segments
101 within a FoV for further analysis.

102 **Locus coeruleus cortical axons signal unsigned visuomotor errors**

103 To determine whether LC axons respond to visuomotor errors, we first measured their responses to
104 visuomotor mismatch stimuli (unexpected 1 s halts of visual flow during locomotion in the closed loop
105 condition). Indeed, LC axons showed significant increases in fluorescence following mismatch
106 presentations (**Figure 1C-D**). Assuming these responses reflect visuomotor prediction errors, we would
107 expect to find two things:

108 First, the responses should depend on precise coupling between visual flow speed and locomotion speed
109 (i.e., when visual flow is predictable from locomotion). Responses to visuomotor mismatch in closed loop
110 conditions should be higher than responses to a replay of the same visual flow halt (termed 'playback
111 halt') in open loop conditions, even when the mouse is locomoting. Playback halts are visually identical to
112 mismatches but occur independent of whether the mouse is stationary or locomoting (**Figure 1A**).
113 Responses of LC axons to playback halts when the mouse was stationary were negative and substantially
114 different from mismatch responses (**Figures 1C-D**), demonstrating that the response of LC axons to
115 visuomotor mismatch cannot be explained by the visual stimulus alone. The mismatch responses also
116 could not be explained by a locomotion driven increase in gain of the visual halt response: a) The average
117 playback halt response when the mouse was stationary was negative, b) there was no correlation between
118 playback halt responses and mismatch responses across different FoVs ($R^2 = 0.04$, $p = 0.31$, 25 FoVs, linear
119 regression), and c) mismatch responses were significantly larger than playback halt responses that

120 occurred during locomotion in the open loop condition (**Figure 1D**). This indicated that responses in LC
121 axons were acutely dependent on visuomotor coupling, since the only difference between a mismatch
122 stimulus and a playback halt during locomotion is that the former occurs during visuomotor coupling and
123 the latter does not.

124 Second, the mismatch response should scale with the size of the error between visual flow speed and
125 locomotion speed, since the latter is a proxy for the prediction of visual flow speed. Since visual flow speed
126 is zero during mismatch, and visual flow is perfectly coupled to locomotion prior to mismatch, the
127 visuomotor error is proportional to the locomotion speed during mismatch (**Figure 1A**). Indeed, we found
128 that LC axonal mismatch responses increased monotonically with the locomotion speed of the mouse
129 (**Figure 1E**). Thus, LC axonal responses to visuomotor mismatch are consistent with a visuomotor
130 prediction error signal.

131 Visuomotor mismatches evoke negative prediction errors because they are a condition where there is *less*
132 visual flow than expected. However, these are not the only type of prediction error in our paradigm. In
133 the open loop condition, visual flow onsets result in positive prediction errors (i.e., a condition with *more*
134 visual flow than expected), especially when the mouse is stationary. We thus assessed the responses of
135 LC axons to visual flow onsets in the open loop condition (i.e., uncoupled from locomotion). We found
136 that LC axons showed significant responses to visual flow onsets, but only when the mouse was stationary
137 (**Figures 1F-G**). Visual flow onsets during locomotion did not evoke significant responses on average.
138 Altogether, LC axonal responsiveness to visual and visuomotor stimuli was best explained by the absolute
139 (i.e., unsigned) error between locomotion and visual flow speeds ($|Error| = |Speed_{locomotion} - Speed_{visual}$
140 $_{flow}|$). Changes in the absolute error resulted in corresponding changes in the activity in LC axons (**Figures**
141 **1C and 1F**), and responses scaled with the size of $\Delta|Error|$ (i.e., the change in unsigned error magnitude,
142 see Methods) across the different stimulus conditions (**Figure 1H**).

143 **Noradrenaline broadcasts visuomotor prediction errors across the dorsal cortex**

144 Individual LC neurons can preferentially target different cortical areas (Chandler et al., 2019; Kebschull et
145 al., 2016), but it is unclear whether these projection-specific neurons have differing response profiles. To
146 assess the heterogeneity of LC signaling across the cortex, we first compared the calcium responses of LC
147 axons between two imaging window locations: the anterior cortex (the primary and secondary motor
148 cortex), and the posterior cortex (V1 and surrounding regions) (**Figure 2A**). We found very similar
149 responses to visuomotor mismatches, playback halts (stationary) and visual flow onsets (stationary)

150 (**Figures 2B and C**), as well as air puffs and locomotion onsets at these two locations (**Figures 2B and D**),
151 and there were no significant differences in the responses between the two locations. These results are
152 consistent with the idea that the LC sends similar visuomotor and locomotion related signals to distinct
153 regions of the cortex, in line with recent findings showing that LC axons in different cortical regions show
154 responses to the same sensory stimuli (Deitcher et al., 2019).

155 **Locus coeruleus axon stimulation has only a small effect on stimulus responses in layer 2/3 of V1**

156 What could be the function of prediction errors signaled by the LC to the cortex? One possibility is that
157 cortical prediction errors, like mismatch responses in V1 (Keller et al., 2012), are enhanced by LC output
158 in order to augment error driven learning. Indeed, a prevalent idea is that noradrenaline is a mediator of
159 gain modulation in the cortex (Ferguson and Cardin, 2020), including the gain increase in V1 during
160 locomotion (Polack et al., 2013). To test whether the LC may enhance prediction error responses in cortical
161 layer 2/3, we assessed the impact of transient LC axon stimulation on cortical responses using an
162 optogenetic strategy (**Figure 3A**). First, we injected an AAV vector encoding Cre-dependent excitatory red-
163 light activated opsin, ChrimsonR, into the right LC of 8 NET-Cre mice, while injecting a vector encoding
164 jGCaMP8m into the right V1 to drive non-specific neuronal expression. An imaging window was then
165 implanted over the right V1. Mice underwent habituation to the virtual reality system before calcium
166 imaging of V1 neurons during 1) a closed loop condition with mismatches and 2) an open loop condition
167 with 1 s fixed-speed visual flow stimuli. During imaging, we stimulated ChrimsonR by directing a 637 nm
168 laser through the objective into the imaging window (27 mW/mm^2, in 15 ms pulses presented at 20 Hz).
169 This stimulation was presented a) alone in closed loop conditions, b) coupled to a random 50% of
170 mismatches (**Figure 3B**), and c) coupled to a random 50% of open loop visual flow stimuli. To assess the
171 visual effects of optical stimulation of ChrimsonR (Danskin et al., 2015) in absence of the effects of
172 optogenetically stimulating LC axons, we also imaged from a second group of 6 mice treated in an identical
173 manner, but without ChrimsonR expression in the LC (control mice). Two mice were excluded from the
174 LC-injected group due to low density of axonal labelling with tdTomato in V1, leaving 6 ChrimsonR-
175 expressing mice in the dataset (see Methods).

176 Optogenetic stimulation, when presented in isolation, resulted in dilations of the right pupil in mice
177 expressing ChrimsonR in a manner that depended on the degree of axon labelling (**Figure 3C and Figure**
178 **S3A**), but not in control mice. This likely resulted from antidromic activation of the LC, direct stimulation
179 of which is known to produce strong ipsilateral pupil dilation (Liu et al., 2017), and increased our

180 confidence that we were indeed driving LC axons with the parameters selected. Onset of the optogenetic
181 stimulation laser caused a small calcium response across the population in ChrimsonR-expressing mice,
182 which was indistinguishable from that caused in control mice (**Figure 3D**). This was likely due to a visual
183 effect of the stimulation laser. The lack of a difference in this stimulation response between ChrimsonR-
184 expressing mice and control mice indicated that optogenetic stimulation of LC axons did not have a direct
185 measurable effect on calcium activity of L2/3 neurons in V1.

186 We then analyzed the effect of optogenetic activation of LC axons on mismatch and visual flow responses
187 of the layer 2/3 population. To take account of visual effects of the laser, we compared the effect of the
188 laser in ChrimsonR-expressing mice with that in control mice. Responses to visual flow onsets (i.e., at the
189 beginning of the visual flow stimulus, or at the offset of mismatch) appeared transiently more pronounced
190 during laser stimulation in ChrimsonR-expressing mice only (**Figures 3E-F**). This was most notable when
191 plotting the difference in average response between trials with concurrent laser stimulation and those
192 without: there were transient increases in response during laser-on trials at visual flow onset, and this
193 effect was significantly different between ChrimsonR-expressing and control groups only during brief
194 time-windows at the onset/resumption of visual flow (**Figures 3E-F**). However, this effect was small and
195 not evident in average responses. Averaging across the full response duration, we found no significant
196 effects of laser stimulation, both when comparing trials with and without laser stimulation in the
197 ChrimsonR-expressing group, and when comparing the difference in response size between ChrimsonR-
198 expressing and control mice (**Figures 3E-F**). No relationship could be found between the degree of LC
199 axonal labelling and the effect of stimulation on average response size, so ChrimsonR expression-level
200 was likely not the limiting factor (**Figure S3B**).

201 In V1, there is electrophysiological and molecular evidence for at least three different layer 2/3 pyramidal
202 neuron types, including negative prediction error (NPE) neurons which respond to visuomotor
203 mismatches, positive prediction error neurons (PPE) which respond to unexpected visual flow (Jordan and
204 Keller, 2020; O'Toole et al., 2022), and an intermediate group. It is therefore conceivable that LC output
205 could have differential effects on these groups that are masked when analyzed at the population level. To
206 quantify potential cell-type specific effects of LC axon stimulation, we thus split the population of neurons
207 into three groups based on locomotion onset responses (see **Figure S4** and Methods): the group with the
208 strongest visuomotor mismatch responses (NPE), the group with the strongest visual flow responses
209 (PPE), and an intermediate population (Other) (**Figure S4**). We found no evidence for an effect of

210 optogenetic stimulation of LC axons on average mismatch and visual flow responses across any of these
211 cell groups (**Figures 3G-H**). We thus concluded that transient LC axon stimulation in the awake state has
212 only a minor direct effect on the responses of neurons in layer 2/3 of V1. These results are largely in line
213 with recent work demonstrating a lack of effect of LC stimulation on baseline firing in cortical pyramidal
214 neurons, and an enhancement of transient responses to afferent input (Vazey et al., 2018).

215 **Phasic LC output enhances sensorimotor plasticity in layer 2/3 of V1**

216 If transient LC activity in the awake state does have a large impact on average layer 2/3 responses directly,
217 what is the function of visuomotor prediction errors signaled by the LC in the cortex? The LC is thought to
218 be involved in cortical plasticity (Kasamatsu et al., 1985; Kasamatsu and Pettigrew, 1976; Martins and
219 Froemke, 2015; Shepard et al., 2015). Catecholamine receptors in V1 are known to modulate synaptic
220 plasticity by activating intracellular signaling cascades and interacting with eligibility traces (Choi et al.,
221 2005; He et al., 2015; Nomura et al., 2014; Seol et al., 2007). One plausible function of LC sensorimotor
222 prediction errors is to gate the plasticity that underlies learning of sensorimotor predictions, e.g., the
223 prediction of visual feedback during locomotion. Primary sensory cortices can indeed learn to suppress
224 the sensory consequences of locomotion, driving selective reductions of responses to locomotion-coupled
225 inputs (Schneider et al., 2018; Widmer et al., 2022).

226 While our optogenetic stimulation of LC axons had only small measurable effects on mismatch or visual
227 flow response size (**Figure 3**), we did notice one striking difference between ChrimsonR-expressing and
228 control mice. In V1, there is a known increase in the size of visual responses during locomotion compared
229 to stationary periods (Bennett et al., 2013; Erisken et al., 2014; Niell and Stryker, 2010; Pakan et al., 2016;
230 Polack et al., 2013; Zmarz and Keller, 2016). Analyzing only trials where the optogenetic stimulation laser
231 was not on, we found that this canonical gain increase was present for control mice but reversed in sign
232 in ChrimsonR-expressing mice: Visual responses during locomotion were suppressed on average relative
233 to stationary periods (**Figure 3I**). This resulted in a significantly lower locomotion modulation index (see
234 Methods) for ChrimsonR-expressing relative to control mice (**Figure 3I**). Since episodic LC axon stimulation
235 occurred throughout the whole imaging session (i.e., across 10 minutes in the closed loop condition, prior
236 to the presentation of open loop visual flow stimuli), it is possible that the reversal of locomotion
237 modulation index reflects a result of plasticity induced by earlier LC axon stimulation.

238 We wanted to directly test the idea that transient LC activation enhances plasticity that leads to a
239 reduction in locomotion modulation index over the course of visuomotor coupling experience. To do this,

240 we designed an experiment to assess the impact of LC axon stimulation on neuronal learning about
241 visuomotor coupling (**Figure 4A**). We expressed jGCaMP8m in neurons in V1 of 19 mice. 12 mice also had
242 AAV vector injections into the LC to express ChrimsonR in NET-positive neurons, while the remaining 7
243 underwent no injection into the LC to serve as controls for the non-optogenetic effects of the protocol.
244 Mice were habituated to the VR as before and we then proceeded to two-photon imaging in layer 2/3 of
245 V1. During the imaging session, mice would first be exposed to 5 minutes of 1 s fixed-speed open loop
246 visual flow presentations, to quantify the gain-change of visual flow responses during locomotion (**Figure**
247 **4A**). Mice were then exposed for 5-10 minutes to either a) a closed loop condition where visual flow and
248 locomotion are coupled, or b) an open loop replay of visual flow generated from a previous closed loop
249 session. During this session, LC axons would be periodically optogenetically stimulated as before (15 ms
250 pulses, presented at 20 Hz for 1 s every 7 seconds on average) to simulate phasic LC responses (**Figure**
251 **4A**). Afterwards, the open loop visual flow presentations would be repeated to quantify how the previous
252 LC axon stimulation affected visual responses. To assess the stimulus specificity with which visual
253 responses changed, we presented both nasotemporal and temporonasal visual flow (mice see the former
254 during forward locomotion in the closed loop condition) (**Figure 4A**). If LC axon stimulation results in
255 enhanced plasticity of locomotion based predictions of visual flow, we would expect the following
256 observations: 1) Suppression of visual flow responses by locomotion is enhanced after stimulation of LC
257 axons in closed loop conditions, 2) this suppression is specific to the type of visual flow seen during
258 forward locomotion (nasotemporal), 3) the effect depends on ChrimsonR expression in the LC, and 4) the
259 effect is absent when LC axons are instead stimulated during open loop conditions (i.e., the effect depends
260 on visuomotor coupling).

261 Optogenetic stimulation caused a degree of pupil dilation that was strongly predictable from axonal
262 ChrimsonR expression levels in V1 quantified postmortem ($R^2 = 0.89$, $p < 10^{-5}$, 12 mice, linear regression)
263 (**Figure 4B**). We split the LC-injected dataset into high ChrimsonR expression (six mice) and low ChrimsonR
264 expression (six mice) according to V1 axonal expression level (**Figures 4B and S5A**). Low ChrimsonR-
265 expressing mice had optogenetically evoked pupil dilations that were not statistically distinguishable from
266 controls, while high ChrimsonR-expressing mice had overt pupil dilations (**Figures 4B and S5B**). For the
267 following analyses, we excluded 8 (5) of 49 (25) sessions from the ChrimsonR (control) dataset due to lack
268 of locomotion during those sessions (see Methods). At the beginning of the imaging session, prior to
269 optogenetic stimulation, neurons in layer 2/3 showed a pronounced positive locomotion modulation
270 index for both the nasotemporal and temporonasal visual flow responses, both in high and low

271 ChrimsonR-expressing mice and in control mice (**Figures 4C-E and S5D**). Quantifying visual flow responses
272 in high ChrimsonR-expressing mice after optogenetic stimulation during closed loop visuomotor
273 experience revealed a significant reduction in the locomotion modulation index for nasotemporal visual
274 flow responses (**Figure 4C**). This originated from a reduction in the response to visual flow during
275 locomotion, while responses during stationary periods remained stable (**Figure 4G**). This effect was
276 specific to the direction of visual flow seen during forward locomotion, since locomotion modulation index
277 was preserved for temporonasal visual flow responses (**Figure 4D**), with negligible changes in response
278 size both during locomotion and stationary periods (**Figure 4H**). The effect was also specific to high
279 ChrimsonR-expressing mice, as locomotion modulation index did not significantly change in both control
280 (**Figure S5D**) and low ChrimsonR-expressing mice (**Figures 4E and 4I**).

281 The selective reduction in locomotion modulation index of nasotemporal visual flow responses in high
282 ChrimsonR-expressing mice could be due to enhanced learning to suppress reafferent visual feedback
283 seen during forward locomotion, or it could simply be due to general exposure to nasotemporal visual
284 flow during optogenetic stimulation (e.g., enhanced adaptation). In the latter case, response size
285 reduction should be the same if optogenetic stimulation takes place during open loop replay of the same
286 visual flow seen during closed loop conditions. To assess this, we repeated the same experiment, but
287 instead of stimulating LC axons during the closed loop condition, we stimulated LC axons during open loop
288 replays of visual flow from previous closed loop sessions of the same mice (**Figure 4A**). Instead of a
289 stimulus selective reduction in locomotion gain, this paradigm drove a nonsignificant increase in
290 locomotion modulation index for both nasotemporal (**Figures 4F and S5F**) and temporonasal visual flow
291 (**Figure S5E**) responses. This confirmed that the reduction in locomotion modulation index after
292 stimulation of LC axons in the closed loop condition (**Figure 4C**) depends on visuomotor coupling
293 experience and is not simply due to exposure to nasotemporal visual flow.

294 We conclude that LC axon stimulation over the course of minutes increases locomotion driven
295 suppression of visual flow responses in layer 2/3 in a manner that is specific to reafferent stimulus
296 properties and dependent on both ChrimsonR expression and visuomotor coupling (**Figure 4J**).
297 Importantly, the effect could not be explained by differences in locomotion behavior between any of the
298 groups analyzed (**Figure S6**).

299 **LC axon stimulation over minutes recapitulates visuomotor plasticity seen over days**

300 In the virtual reality environment, mouse movement and visual flow are constrained to the forward-
301 backward dimension, and the visuomotor gain is constant: changes in visuomotor gain that would usually
302 occur during changes in environment geometry are absent. Mice head-fixed in the VR therefore
303 experience a vastly reduced diversity of visuomotor coupling compared to freely moving conditions. The
304 reduction in locomotion modulation index resulting from LC axon stimulation (**Figure 4C**) may therefore
305 result from overlearning of this simplified visuomotor coupling.

306 If this interpretation is correct, then extensive training within the VR should also lead to visual flow
307 response suppression during locomotion even in mice without artificial LC axon stimulation. To assess this
308 idea, we reanalyzed two-photon calcium imaging data from V1 layer 2/3 in coupled trained mice reared
309 with visual experience entirely constrained to that of the visuomotor coupling in the VR across days (and
310 otherwise dark reared) (Attinger et al., 2017; Widmer et al., 2022) (**Figure 5A**). We compared this data to
311 similar data from normally reared mice that also have experience of the virtual reality system, but that
312 had experience of normal visuomotor coupling in freely moving conditions (Vasilevskaya et al., 2022;
313 Zmarz and Keller, 2016) (**Figure 5A**). Analyzing responses to nasotemporal visual flow onsets during open
314 loop replay, we found that visual flow responses were amplified during locomotion relative to stationary
315 periods in normally reared mice but were suppressed during locomotion in coupled trained mice (**Figure**
316 **5B**). This resulted in a significantly lower locomotion modulation index in coupled trained mice compared
317 to normally reared mice (**Figure 5C**). The effect was not due to dark rearing, as non-coupled trained mice
318 (also dark reared, but with only open loop virtual reality experience (**Figure 5A**) (Attinger et al., 2017))
319 showed a positive locomotion modulation index on average that did not significantly differ from that of
320 normally reared mice (**Figure 5C**).

321 Qualitatively, the comparison of locomotion modulation index between normally reared and coupled
322 trained mice (**Figures 5B-C**) was similar to the change in locomotion modulation index in ChrimsonR-
323 expressing mice for nasotemporal visual flow after LC axon stimulation (**Figure 4C**). This suggests that the
324 increase in locomotion driven suppression after LC axon stimulation is caused by a similar form of plasticity
325 to that seen when visuomotor experience is constrained to the virtual reality across days. If this is the
326 case, we should see similarities in the properties of the locomotion driven suppression. First, we looked
327 at the locomotion speed dependence of the suppression. If the negative locomotion modulation index
328 results from learning to suppress visual responses according to a locomotion driven prediction of visual

329 flow, the degree of suppression should depend on locomotion speed. As locomotion speed increased,
330 visual flow responses were increasingly suppressed in coupled trained mice (**Figure 5D**), while this was
331 not evident in normally reared mice (**Figure 5E**). For nasotemporal visual flow responses in ChrimsonR-
332 expressing mice, locomotion modulation index was positive and did not change with locomotion speed at
333 the start of the imaging session, but after stimulation of LC axons in closed loop conditions, locomotion
334 modulation index became increasingly negative as locomotion speed increased (**Figure 5F-G**). Thus, the
335 locomotion driven suppression of visual flow emerging after stimulating LC axons in closed loop conditions
336 was locomotion speed dependent in a similar manner to the locomotion driven suppression seen in
337 coupled trained mice. Note that in high ChrimsonR-expressing mice, suppression of visual flow was seen
338 at high locomotion speeds only (**Figure 5G**), but in coupled trained mice, some level of suppression was
339 evident across all speeds (**Figure 5E**). This could be due to differences in visual flow speed: for coupled
340 trained mice, the stimuli analyzed are visual flow onsets during open loop replay; thus, the visual flow
341 speed will cover a similar range as the locomotion speed distribution of the mice. For high ChrimsonR-
342 expressing mice, the stimuli are presented at a fixed visual flow speed that often exceeds the locomotion
343 speed of the mouse. Thus, the fact that suppression only appears at the highest locomotion speed in these
344 mice is consistent with a suppression of visual flow input based on a locomotion speed dependent
345 expectation. In addition to the similarities in locomotion speed dependence of suppression in the two
346 groups, the pattern of change in locomotion modulation index across different functional layer 2/3 cell
347 groups also appeared similar between high ChrimsonR-expressing and coupled trained mice (**Figure S7**).

348 Overall, the pattern of differences in locomotion modulation was remarkably similar for ChrimsonR-
349 expressing (**Figures 5G, and S7D**) and coupled trained mice (**Figures 5E and S7B**). This indicates that the
350 functional consequence of plasticity evoked by minutes of LC axon stimulation during visuomotor coupling
351 is similar to that seen after experience is developmentally constrained to visuomotor coupling for days.

352 DISCUSSION

353 The locus coeruleus (LC) has long been hypothesized by computational models to report quantities such
354 as unexpected uncertainty (Yu and Dayan, 2005) or high level state-action prediction errors (Sales et al.,
355 2019). What these quantities have in common is that they essentially are metrics for the inaccuracy of the
356 brain's internal models. One way to implement such a measure would be to integrate prediction errors
357 from across the brain and then broadcast this signal back across the brain. Indeed, we found that the LC

358 sends unsigned visuomotor prediction errors non-specifically across the dorsal cortex (**Figures 1 and 2**).
359 Models hypothesizing that the LC reports the global inaccuracy of the brain's internal models suggest that
360 the purpose of this is to increase learning rates in output circuits like the cortex, enabling internal models
361 to be modified more rapidly. In line with this, we found that stimulating cortical LC axons during closed
362 loop visuomotor coupling over minutes reduces and even reverses the canonical locomotion related gain
363 of visual flow responses in layer 2/3 of V1, in a manner specific to the direction of the movement-coupled
364 stimulus (**Figure 4**). Surprisingly, this enhanced plasticity seems to happen even with only a small direct
365 effect of LC axon stimulation on average calcium responses (**Figure 3**). This plasticity, on the timescale of
366 minutes, recapitulates the effect of restricting visuomotor experience to the closed loop coupling in virtual
367 reality across days (**Figure 5**), suggesting that it reflects an acceleration of a slower form of visuomotor
368 plasticity (i.e., an increased learning rate).

369 The LC responds to unexpected stimuli of various modality, including reward prediction errors,
370 punishment prediction errors, and novel or intense unexpected sensory stimuli (Aston-Jones and Bloom,
371 1981; Basu et al., 2022; Bouret and Sara, 2004; Breton-Provencher et al., 2022; Deitcher et al., 2019; Foote
372 et al., 1980; Hervé-Minvielle and Sara, 1995; Su and Cohen, 2022; Takeuchi et al., 2016; Vankov et al.,
373 1995). The responses we found in LC axons to the various visual flow stimuli were proportional to the
374 change in the degree of error between visual flow and locomotion speeds (**Figure 1**). This supports a model
375 in which the LC signals prediction errors, and combined with previous findings, suggests that prediction
376 errors of all modalities are a general feature of LC signaling. Both positive and negative visuomotor
377 prediction errors appear to be computed in layer 2/3 of the primary visual cortex (Jordan and Keller, 2020)
378 and activate the anterior cingulate cortex (Heindorf and Keller, 2022) – an area that projects directly to
379 the LC. Thus, the LC likely inherits prediction errors computed upstream in areas like the cortex. Based on
380 the multimodality and unsigned nature of LC responses, and the integrate and broadcast nature of its
381 input-output anatomy (Schwarz et al., 2015), our working model of LC function is as follows: The LC
382 integrates prediction errors of all modalities to compute a measure of how inaccurately internal models
383 are currently predicting the global sensory inputs of the animal. The LC does not signal what *type* of
384 prediction error occurred, but what the global rate of prediction errors currently is (i.e., a measure of
385 surprise). The resulting LC output does not directly *drive* model updating in cortical output areas, but it
386 modulates the rate at which local cortical prediction errors drive plasticity in internal models. Thus, the
387 specificity of how internal models are changed depends on ongoing prediction errors in the cortex, and
388 the LC input acts to control the learning rate, modulating the extent to which these cortical prediction

389 errors drive plasticity. This would allow the LC to be a controller of plasticity in internal models: when
390 prediction error rates are high (i.e., during developmental, novel, or volatile situations), updating of
391 internal models will be more rapid as a result of increased LC output. To support this hypothesis, it is
392 important for future work to expand the range of LC stimulation parameters tested to identify the function
393 between LC activation level and cortical plasticity, as well as cortical representations.

394 While the idea of a brain wide average over sensory prediction errors can explain many of the observed
395 LC responses, other responses are less easily explained by prediction error. LC calcium responses to
396 locomotion onsets, which have been shown previously in LC axons (Deitcher et al., 2019; Reimer et al.,
397 2016), were generally larger than visual flow or visuomotor mismatch responses (**Figures 2 and S2**). This
398 could be the result of a direct movement related input unrelated to prediction errors, or the result of
399 prediction errors that are not driven by differences between forward locomotion and backward visual
400 flow. Increases in activity occurring after locomotion onset could reflect vestibulomotor prediction errors
401 that result from the fact that the mouse is head-fixed, or visuomotor prediction errors for motor attempts
402 we do not record, like turns or head movements. We do find that visuomotor prediction errors contribute
403 to locomotion onset responses, as locomotion onset responses in the open loop condition are smaller
404 during visual flow, when locomotion evoked visuomotor error is lower (**Figure S2B**). However, LC calcium
405 activity also rises prior to locomotion onset, creating the additional possibility of an internally generated
406 movement onset response. Other kinds of movement are also correlated with LC firing, including pup
407 retrievals (Dvorkin and Shea, 2022) and lever pressing (Breton-Provencher et al., 2022). These movement
408 onset responses could also reflect other forms of prediction error, including action prediction errors
409 (Greenstreet et al., 2022) or temporal difference reward prediction errors (in cases where the movement
410 is associated with reward expectation) similar to those documented in the dopaminergic system (Kim et
411 al., 2020). Future work will need to investigate these possibilities to build a complete general model of LC
412 computation.

413 Depleting noradrenaline has been shown to prevent forms of sensory-guided developmental plasticity in
414 the cortex, including ocular dominance plasticity in V1 (Kasamatsu and Pettigrew, 1976) and changes in
415 the tonotopic map in the auditory cortex (Shepard et al., 2015). Loss of function experiments can suffer
416 from the potential confound that catecholamines may simply be necessary for normal neuronal activity,
417 and the loss of plasticity may be a secondary effect of a disruption in neuronal function. Indeed, acute
418 noradrenergic receptor block can silence neurons in layer 2/3, and massively reduce the amplitude of

visual inputs (Polack et al., 2013). In gain of function experiments, electrical stimulation of the LC has been shown to partially restore ocular dominance plasticity in adult cats (Kasamatsu et al., 1985). Here we also performed a gain of function experiment: we show that a few minutes of optogenetic LC axon stimulation in V1 of adult mice during visuomotor coupling can recapitulate the developmental effects of constrained exposure to visuomotor coupling in the virtual reality (**Figures 4 and 5**). While our optogenetic stimulation is likely far more constrained to LC neurons than previous electrical stimulations, we cannot rule out a systemic effect of the LC axon stimulation. We know that we are likely antidromically activating the LC with our optogenetic stimulation owing to the resulting pupil dilation (**Figures 3C and 4B**). Given that LC neurons are electrically coupled (McKinney et al., 2022) and have widely divergent axons, our stimulation likely has effects on other LC output targets, such as other neuromodulatory systems, and other areas of the cortex. Thus, the plasticity effect that we measure may not entirely result from LC output in V1 alone. However, since the LC will never be acting in isolation and broadcasts its output to different cortical areas, the functional impact of LC axon stimulation in this experiment is strongly suggestive of a role in facilitating plasticity. Future work will be needed to understand the circuit locus of plasticity generated by this paradigm, and its dependence on particular neuromodulators (e.g., dopamine and noradrenaline). The fact that the plasticity occurs despite only minor effects of LC stimulation on neuronal activity (**Figure 3**) indicates that the LC can either enhance plasticity without effecting activity levels, for instance via the molecular cascades or eligibility traces activated by GPCRs (He et al., 2015; Hong et al., 2022; Seol et al., 2007), and/or that a part of the relevant circuit outside of layer 2/3 is more strongly modulated by LC activation.

Locus coeruleus activation has been shown to facilitate learning rates at the behavioral level (Glennon et al., 2023, 2019; Martins and Froemke, 2015). The behavioral relevance of the LC-gated plasticity in our study is yet to be demonstrated, but we can conjecture some perceptual functions of the plasticity based on its nature: learned suppression of reafferent visual flow during locomotion. This theoretically would be useful at the perceptual level for detection of external moving objects during movement, or for detecting changes in the geometry of the environment through which the animal is moving. Novel behavioral paradigms for assessing these percepts could be used in future studies to demonstrate the behavioral impact of the plasticity that we see.

Prediction error driven catecholamine release is thought to gate cortical synaptic plasticity during reinforcement learning (He et al., 2015; Roelfsema and Holtmaat, 2018). The results presented here

449 expand this idea from reward associations to sensorimotor associations. We propose that a general
450 function of catecholamines is to gate the plasticity underlying predictive learning across all modalities.

451 AUTHOR CONTRIBUTIONS

452 RJ designed and performed the experiments and analyzed the data. Both authors wrote the manuscript.

453 ACKNOWLEDGEMENTS

454 We thank all members of the Keller lab for discussion and support, Tingjia Lu for the production of viral
455 vectors, Susumu Tonegawa for sharing NET-Cre mice, and Andreas Lüthi for reagents and equipment. This
456 project has received funding from Human Frontier Science Program (LT000077/2019-L, long term
457 fellowship to RJ), the Swiss National Science Foundation, the Novartis Research Foundation, and the
458 European Research Council (ERC) under the European Union's Horizon 2020 research and innovation
459 programme (grant agreement no. 865617).

460 DATA AND CODE AVAILABILITY.

461 All data and analysis code are available at https://data.fmi.ch/PublicationSupplementRepo/.

462 METHODS

463 **Animals and husbandry.** Mice used in the study were of the NET-Cre strain (Wagatsuma et al., 2018) bred
464 in-house, either heterozygous transgenics or (in the case of some controls) wild types. Both males and
465 females were used, and all mice were aged between 8 and 20 weeks. Mice had ad libitum access to water
466 and regular mouse chow throughout the entire study. Mice were co-housed in groups of 2 to 5 in a
467 reversed 12-hour light-dark cycle, and all imaging experiments took place during the dark part of the cycle.

468 **Viral vector injections and surgery.** All animal procedures were approved by and carried out in
469 accordance with guidelines of the Veterinary Department of the Canton Basel-Stadt, Switzerland. For all
470 surgical procedures, mice were anesthetized with an intraperitoneal injection of a mixture of fentanyl
471 (0.05 mg/kg), medetomidine (0.5 mg/kg), and midazolam (5 mg/kg) and provided with both peri- and
472 postoperative general analgesics: Metacam (5mg/kg, s.c.) and buprenorphine (0.1 mg/kg, s.c.). A lidocaine
473 and ropivacaine mixture was injected subcutaneously into the scalp prior to incision. Metacam analgesia

474 was provided for a further 48 hours post-surgery. Mice were allowed to recover for 1-3 weeks prior to
475 first head-fixation.

476 **Surgeries for two-photon imaging of LC axons.** 13 male and female NET-Cre mice (4-6 weeks old) were
477 unilaterally injected at stereotactic coordinates (relative to bregma and brain surface): 5.45 mm posterior,
478 1.10 mm lateral, 3.65 mm deep. 250 to 500 nl of AAV2/5-hSyn-DIO-axon-GCaMP6s (2.7 x 10^{13} genome
479 copies/ml) was injected into each site. A 4 mm diameter circular imaging window was then implanted. A
480 circular craniotomy was made overlying visual cortex (8 mice) or motor cortex (4 mice) and a durectomy
481 was performed. A glass window was then placed onto the craniotomy and fixed in place with
482 cyanoacrylate. A custom titanium headplate was attached to the skull using dental cement (Paladur,
483 Kulzer).

484 **Surgeries for two-photon imaging in layer 2/3 V1 during optogenetic stimulation of LC axons.** Male and
485 female NET-Cre mice (4-6 weeks old) were unilaterally injected with 250 to 500 nl of AAV2/1-hSyn-DIO-
486 ChrimsonR-tdTomato (1.2 x 10^{13} to 3.4 x 10^{13} genome copies/ml) into the right LC at stereotactic
487 coordinates (relative to bregma and brain surface): 5.45 mm posterior, 1.10 mm lateral, 3.65 mm deep. A
488 maximum of 250 nl of AAV2/1-hSyn-soma-jGCaMP8m (titer range from 10^{13} to 10^{15} genome copies/ml)
489 was then injected across 3-5 locations spanning right V1, and a window and headplate were implanted as
490 above, but with the additional measure of black pigmenting of the dental cement for the reduction of
491 optogenetic stimulation light reaching the eyes of the mouse. For control mice, the injection into the LC
492 was omitted. For the dataset in **Figure 3**, eight mice were injected in the LC, but two were excluded due
493 to lack of expression (see section Axon density). Six mice were not injected in the LC to serve as controls.
494 For the dataset in **Figure 4**, 12 mice were injected in the LC, with 6 mice classified as high ChrimsonR-
495 expressing and 6 mice classified as low ChrimsonR-expressing (see section Axon Density). 7 mice were not
496 injected in the LC to serve as controls.

497 **Immunohistochemistry**. For all experiments with vector injections in LC to express either GCaMP or
498 ChrimsonR-tdTomato, we histologically verified that expression was confined to the neurons within the
499 anatomical location and spatial pattern expected of the LC. In a subset of mice used for imaging LC axons,
500 we also confirmed that the transgene expressing neurons were catecholaminergic by immunostaining for
501 tyrosine hydroxylase and GFP (**Figure S1A**). After transcardial perfusion, brains were extracted and placed
502 in 4% paraformaldehyde overnight. Brains were then embedded in 4% agar and sliced at 40 µm on a
503 vibratome. Free floating slices were then washed in PBS-triton, blocked for 2 hours with 10% goat serum,

504 and incubated overnight with primary antibodies (1:1000 dilution rabbit anti-tyrosine hydroxylase (Sigma
505 Aldrich 657012), and 1:500 dilution chicken anti-GFP (Abcam ab13970)). The following day, slices were
506 washed again in PBS-triton and incubated for 2 hours with the secondary antibodies at 1:1000 dilution
507 (Alexa Fluor 488 anti-chicken (Jackson ImmunoResearch 703-545-155) and Alexa Fluor 568 anti-rabbit
508 (ThermoFisher Scientific, A10042)). Slices were mounted in Fluoroshield with DAPI (F6057, Sigma Aldrich).

509 **Virtual reality and visual stimuli.** A virtual tunnel, with walls patterned with vertical sinusoidal gratings
510 was projected onto a toroidal screen spanning 240 degrees horizontally and 100 degrees vertically of the
511 visual field. The projector output was gated by a 24 kHz TTL such that it only turned on at the turnaround
512 points of the two-photon resonance scanner, minimizing light artifacts during imaging. Mice were head-
513 fixed on an air-floated polystyrene ball of 20 cm diameter. Movement of the virtual tunnel walls could
514 occur only in one dimension (forward and backwards), with the ball restricted to rotation around the pitch
515 axis using a pin. In closed loop conditions, visual flow speed in the tunnel was coupled to the rotation of
516 the ball, with the exception of brief 1 s mismatch stimuli. These were triggered every 12 ± 2 s (mean ± SD)
517 regardless of locomotion behavior and would clamp the visual flow speed to zero. In open loop conditions,
518 the visual flow speed was controlled irrespective of mouse locomotion. Three different types of open loop
519 session were used: 1) for LC axon imaging (**Figures 1 and 2**), as well as optogenetic stimulation of LC axons
520 during open loop replays (**Figure 4**), the visual flow from a previous closed loop session would be replayed.
521 For LC axon imaging, the visual flow onset responses and playback halt responses were analyzed during
522 this session. 2) For stimulation of LC axons to assess the effect on cortical responses (**Figure 3**), 1 s fixed
523 speed nasotemporal visual flow stimuli would be presented every 9 ± 3 s (mean ± SD). We presented 3
524 different speeds of visual flow in a pseudorandom order. 3) For assessing the effects of LC axon stimulation
525 on visuomotor plasticity (**Figure 4**), we presented 1 s duration fixed speed visual flow stimuli every 7 ± 1 s
526 (mean ± SD), but this time only one speed was presented (equivalent to the speed seen during 24 cm/s
527 locomotion in closed loop conditions), however, the direction was either nasotemporal or temporonasal,
528 in a pseudorandom order. All mice imaged were habituated to head-fixation and the virtual reality tunnel
529 for at least four daily one-hour sessions prior to imaging, until they showed regular, comfortable
530 locomotion.

531 **Two-photon imaging.** Imaging was performed on a modified Thorlabs Bergamo II two-photon microscope
532 system. Excitation illumination was provided by a Ti-Sapphire laser with a wavelength at 930 nm and a
533 laser power between 20 and 30 mW under the objective. When imaging neurons in V1, a piezo scanner

534 was used to move the objective to image 4 separate layers sequentially (15 Hz effective frame rate), but
535 for LC axons, imaging was fixed in a single layer (60 Hz frame rate). Field of view size was 750 × 400 pixels
536 (approximately 300 x 300 µm). Custom software was used to acquire the imaging data. For mice
537 undergoing imaging of layer 2/3 V1 neurons (**Figures 3 and 4**), two-photon imaging sites were confirmed
538 as being in V1 by mapping V1 boundaries using intrinsic signal optical imaging.

539 **Optogenetic stimulation of LC axons.** The beam from a 637 nm OBIS laser (Coherent) was focused onto
540 the imaging site via the two-photon microscope objective. The laser was gated to turn on only during the
541 turnaround times of the two-photon resonance scanner, to minimize stimulation induced light artifacts.
542 During stimulation, the laser was presented in 15 ms pulses at 20 Hz (30% duty cycle) for a total duration
543 of 1 s. For stimulation during visual stimulus presentations (**Figure 3**), the power was 27 mW/mm^2. Since
544 this evoked a small visual response in the V1 calcium activity of both ChrimsonR-expressing and control
545 mice (**Figure 3C**), the power was reduced for subsequent experiments to 20 mW/mm^2 (**Figure 4**), at which
546 point the positive visual response disappeared (**Figure S5C**). For the optogenetic stimulation during visual
547 stimulus presentations (**Figure 3**), optogenetic stimulation occurred simultaneous with a random 50% of
548 mismatch stimuli and visual flow stimuli, or in isolation, every 12 s on average, during closed loop
549 conditions. For optogenetic stimulation in the plasticity experiments (**Figure 4**), stimulation occurred
550 every 7 s on average. In 17/61 included imaging sites, this was gated by mouse locomotion such that
551 stimulation only occurred when locomotion speed exceeded 4 cm/s. Since the results looked very similar
552 for both locomotion gated and ungated stimulations, the data were pooled for analysis.

553 **ΔF/F calculation.** Raw images were full-frame registered to correct for lateral brain motion. For V1 layer
554 2/3 neurons, neuronal somata were manually selected based on mean and maximum fluorescence
555 images. Average fluorescence per region of interest (ROI) was corrected for slow fluorescence drift over
556 time using an 8th percentile filter and a 1000 frame window, and divided by the median value over the
557 entire trace to calculate ΔF/F (Dombeck et al., 2007). For LC axonal data (**Figures 1 and 2**), there were a
558 number of alternative/additional steps. First, all ROIs within an image above a manually set fluorescence
559 threshold were selected. Non-axonal ROIs from this set were then removed in two ways: first, a 'circularity
560 index' (circularity index = 4π x area/perimeter^2) and area threshold were used. ROIs with circularity index
561 above 0.14 or a total area below 150 pixels were excluded – this served to remove non-axonal structures.
562 Second, any ROI without evidence of calcium activity was removed: a fast Fourier transform was used to
563 obtain the power spectrum of the ΔF/F trace. From this, the signal-to-noise ratio of the calcium signal was

564 calculated, where noise was calculated as the average power between 3 and 8 Hz. ROIs with power below
565 a signal-to-noise ratio of 10 in the frequency band from 0.05 to 1 Hz (classified as signal) were excluded.
566 This served to remove uncommon elongated non-axonal ROIs, such as blood vessel walls. Next, due to the
567 lower signal to noise of the axonal recordings, the ΔF/F recorded at 60 Hz was low pass filtered at 10 Hz.
568 Finally, due to the high correlation of ΔF/F between LC axonal ROIs within a field of view (**Figure S1D-F**),
569 ΔF/F was averaged across all axonal ROIs within a field of view.

570 **Calculation of visuomotor error (Figure 1).** Visuomotor error is calculated as the difference between
571 locomotion speed and visual flow speed, assuming a constant gain between the two that the mouse
572 predominantly experiences in the virtual reality. The change in absolute error (Δ|Error|) is calculated for
573 each trial as the change in absolute (i.e., unsigned) visuomotor error during the stimulus window, minus
574 the absolute visuomotor error in the 1 s preceding the stimulus. For each type of stimulus and each FoV,
575 Δ|Error| was then averaged across trials. Note that for visuomotor mismatch, Δ|Error| is equivalent to
576 the locomotion speed during mismatch (since visual flow speed during mismatch is zero, and the
577 preceding 1 s is closed loop, where the error is zero). In all stimulus conditions (**Figure 1H**), the Δ|Error|
578 is calculated in a window 0.66 s (40 frames) preceding the window used to calculate ΔF/F responses.

579 **Locomotion onsets and visual flow onsets.** Locomotion onsets were defined as the locomotion speed
580 crossing a threshold of 0.4 cm/s, where the average speed in the previous two seconds was < 0.4 cm/s,
581 and where the average speed in the subsequent 1 s exceeded 2 cm/s. The same criteria were used to
582 determine visual flow onsets during open loop replays, using the visual flow speed.

583 **LC axonal responses.** For each visual stimulus trigger, the average ΔF/F in the 1 s window prior to stimulus
584 onset was subtracted from the response, before averaging across trials to get the average response of
585 each axon segment. Mismatch and playback halt responses were calculated for each FoV in the 1 s window
586 beginning 0.66 s (40 frames) after stimulus onset. For visual flow onsets during open loop replays, the
587 window was delayed by 400 ms (25 frames) to take into account the slower onset of the stimulus
588 compared to mismatches. Trials were classified as occurring during locomotion if the locomotion speed
589 in the 1 s after the onset of visual flow or mismatch exceeded 1 cm/s, while they were classified as
590 occurring during stationary periods if the locomotion speed was below 1 cm/s. For **Figure 1H**, fast
591 locomotion during mismatch was classified as locomotion speed exceeding 10 cm/s, while slow
592 locomotion was classified as locomotion speed between 1 cm/s and 10 cm/s. For locomotion onset
593 responses (**Figure S2**), the average ΔF/F in the 500 ms window 2 s prior to locomotion onset was

subtracted from the response, before averaging across trials. Locomotion onsets were considered to take place during the absence of visual flow if average visual flow speed in the 2 s window centered on locomotion onset was below that corresponding to a 1 cm/s locomotion speed in closed loop conditions. If visual flow speed exceeded this value, the trial was considered to take place during visual flow. Responses for all stimuli were averaged for each FoV across trials only if there were at least three valid trials. For all stimulus conditions that were selected based on locomotion speed (e.g., mismatches), 120 sham triggers were generated and sham responses calculated from triggers that were sub-selected based on the same locomotion selection criteria. The average sham response was subtracted from the stimulus response.

V1 layer 2/3 neuron stimulus responses. For each stimulus trigger, the average ΔF/F in the 1 s window prior to stimulus onset was subtracted from the response, before averaging across trials to get the average response of the neuron. Visual flow and mismatch responses were calculated for each neuron in the window 0.33 s to 2.33 s (5 to 30 frames) after stimulus onset. Trials were classified as occurring during locomotion if the locomotion speed in the 1 s during visual flow or mismatch exceeded 4 cm/s, while they were classified as during stationary periods if the locomotion speed was below 1 cm/s. For mismatches, only locomotion trials were included. Note that for **Figure 3**, visual responses were not segregated into locomotion and stationary trials: all trials were included. For analysis of locomotion modulation index in different locomotion speed conditions (**Figures 5D-G**), slow, medium, and fast locomotion speed trials were categorized where average locomotion speed during visual flow was between 1 and 5 cm/s, 5 and 10 cm/s, and above 10 cm/s respectively. For the previously published datasets (**Figure 5**, CT, NR, and NT) (Attinger et al., 2017; Vasilevskaya et al., 2022; Widmer et al., 2022), differences in the measurement of locomotion speed across the datasets made it difficult to use a common threshold value. Thus, to make the locomotion modulation indices comparable to those calculated from the newly acquired dataset (**Figures 5D-G**), we used the 95th percentile of the locomotion speed to normalize thresholds across datasets. In addition, since the visual responses used to measure locomotion modulation index were visual flow onsets in open loop conditions rather than rapid onset fixed speed stimuli, the analysis window relative to stimulus onset was shifted by 400 ms to account for the slower onset. Responses were averaged for each neuron across trials only if there were at least three valid trials. For all stimulus conditions that were selected based on locomotion speed (e.g., mismatches), the average response to 1000 sham triggers sub-selected based on the same locomotion conditions was calculated. This sham response was subtracted from the stimulus response.

625 **Locomotion modulation index.** To quantify the change in mean visual flow response during locomotion
626 for each neuron normalized by the overall size of response, we calculated a locomotion modulation index
627 (LMI) for each neuron as follows:

628 $$LMI = \frac{R_{VFloco} - R_{VFstat}}{\sqrt{{R_{VFloco}}^2 + {R_{VFstat}}^2}}$$

629 Where R_{VFloco} is the average visual flow response during locomotion, and R_{VFstat} is the average visual flow
630 response during stationary periods.

631 **Exclusion criteria in analysis of visual plasticity (Figure 4).** Imaging sessions during which the mouse spent
632 less than 15% of the time locomoting at a speed exceeding 4 cm/s were excluded (13 of 71 sessions), as
633 this would limit both the amount of visuomotor coupling experienced during the plasticity assay, and our
634 ability to analyze visual responses during locomotion.

635 **Layer 2/3 functional cell type classification (Figure S4).** Neurons were grouped into visually suppressed
636 and mismatch activated NPE neurons, visually activated PPE neurons, and an intermediate group ('other').
637 Since we were analyzing the visual and mismatch responses of these groups, we used locomotion onset
638 responses to group neurons to avoid a circular analysis. To compute each neuron's locomotion onset
639 response, for each onset the average ΔF/F in the 1 s window beginning 2 s prior to locomotion onset was
640 subtracted from the response, before averaging across trials. Average responses to locomotion onsets
641 (quantified in the window 0.66 to 4 s (10 to 60 frames) after onset) in open loop conditions were
642 subtracted from locomotion onset responses in closed loop conditions (where visual flow is concurrent
643 with locomotion) for each neuron. Note that for analyzing the dataset in **Figure 4**, only the open loop
644 locomotion onsets before LC axon stimulation were used. It was previously shown that the difference
645 between locomotion onset responses in open and closed loop conditions correlates with these cell groups
646 (Jordan and Keller, 2020). For each dataset, the 33rd and 66th percentile of these values were used as
647 thresholds. Neurons with response differences exceeding the 66th percentile were classified as PPE
648 neurons, and those with response differences below the 33rd percentile were classified as NPE neurons,
649 with the remaining neurons were classified as 'other'. Responses to mismatch and visual flow stimuli were
650 consistent with these groupings in all three datasets (**Figure S4**).

651 **Axon density.** PFA fixed brains of mice injected with a vector to express ChrimsonR-tdTomato in NET-
652 positive neurons of the LC were sliced at 40 µm and after mounting, examined under a confocal

653 microscope at 20x magnification. For all mice, images were taken from four sites in V1, each one from a
654 different cortical slice, with sites chosen based on somatic labelling in the green channel (indicating
655 GCaMP expression and a likely two-photon imaging site). To quantify LC axon density, the red channel
656 images were then analyzed. tdTomato labelled axonal segments were manually traced in ImageJ using the
657 NeuronJ plugin (Meijering et al., 2004). The total combined length of the axon segments was then divided
658 by the total area of the cortex in the image to calculate axon density in each image. The average density
659 across four images was taken as the axon density for each mouse. This value was used to distinguish high
660 expression and low expression mice based on a threshold of 0.002 µm per μm^2 (total axon length per unit
661 area of the cortex) (**Figures 4B and S5A**). Since only two mice were categorized to have low expression in
662 the dataset used in **Figure 3**, low expression mice were not included as a separate group in these analyses,
663 and instead excluded.

664 **Pupillometry.** Images of the right eye, ipsilateral to the side of LC stimulation, were recorded with a CMOS
665 infrared camera at 30 Hz. Pupil diameter was measured offline by fitting a circle to the pupil, which was
666 backlit by the 930 nm laser light of the two-photon microscope. Pupil diameter traces were z-scored by
667 subtracting the mean of the entire trace and dividing by the standard deviation of the entire trace. To
668 calculate optogenetically induced pupil dilations, the average baseline pupil diameter (in the 1 s prior to
669 stimulus onset) was subtracted from the response for each trial, then the pupil diameter response was
670 averaged across trials. Trials including blinks were excluded.

671 **Statistical tests.** All statistical information for the tests performed in this manuscript are provided in **Table**
672 **S1**. For data where the experimental unit was neurons, we used hierarchical bootstrapping (Saravanan et
673 al., 2020) for statistical testing due to the nested structure (neurons and mice) of the data. To do this, we
674 first resampled the data (with replacement) at the level of imaging sites. From the selected set of imaging
675 sites, we then resampled the data (with replacement) at the level of neurons. We then computed the
676 mean of this bootstrap sample. This would be repeated 10 000 times to generate a distribution of mean
677 values. For paired tests, the p-value was calculated as the proportion of this distribution that was higher
678 or lower than zero, depending on the null hypothesis. For unpaired tests, the p-value was calculated as
679 the proportion of the distribution higher or lower than the values from the distribution of the compared
680 dataset, depending on the hypothesis. For the bootstrap tests for negative regression slopes (**Figure 5E**
681 **and 5G**), the slope of the linear regression fit was calculated for the 10 000 bootstrapped datasets, and
682 the p-value was taken as the proportion of the distribution with a linear regression fit slope exceeding

683 zero. For data where the experimental unit was FoV (**Figures 1 and 2**) or mice (pupil dilation, **Figure S5B**),
684 t-tests were used to compare datasets that conformed with normality and did not show statistically
685 distinguishable variances. Datasets that did not conform with normality or had unequal variances were
686 compared with Rank-sum tests. Paired t-tests were used to test the mean of a population against zero
687 when the data was normally distributed, otherwise signed-rank tests were used to test the median against
688 zero (**Figure 1**).

689

690 **MAIN FIGURES**

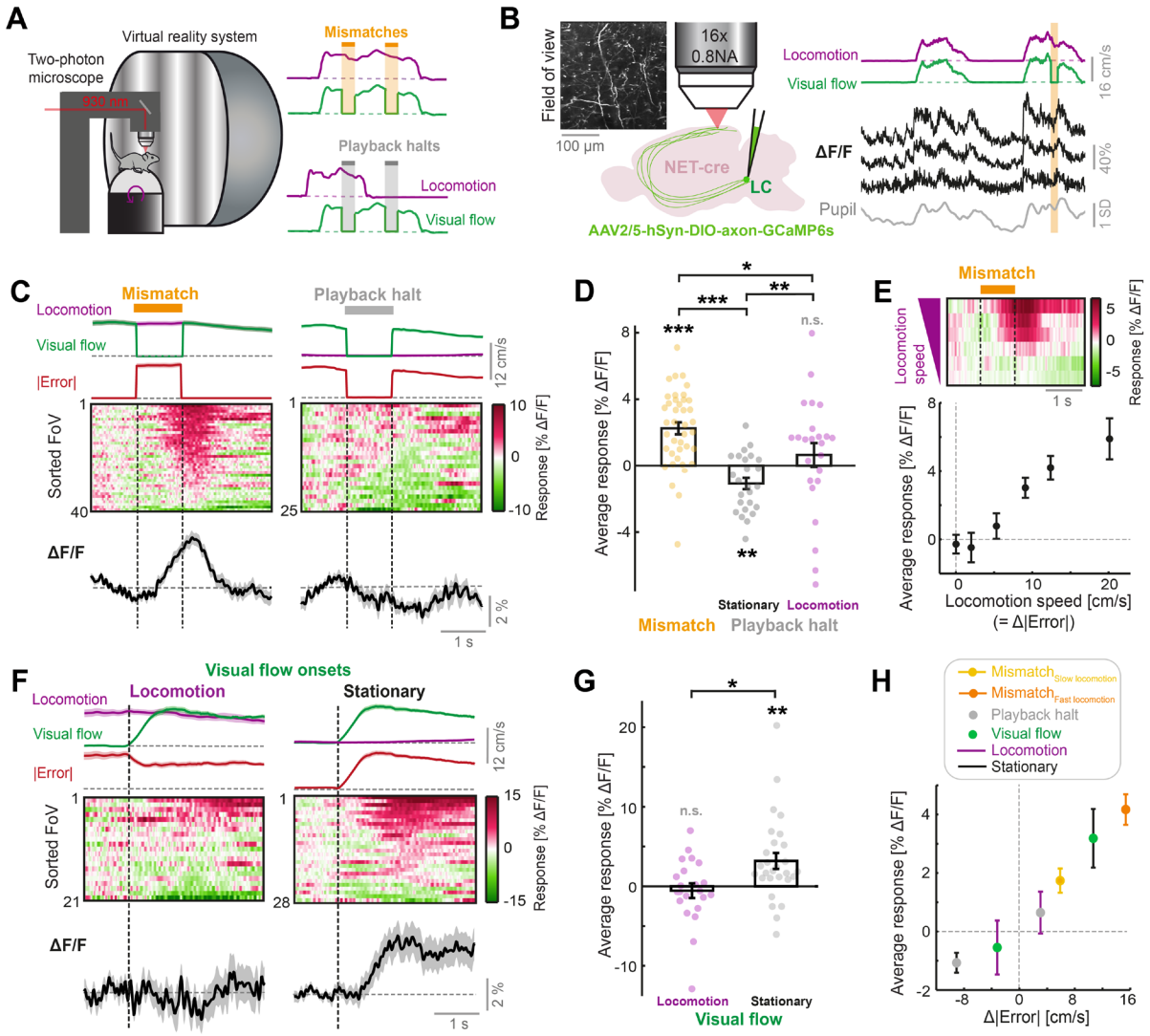

691

692 **Figure 1. LC axonal calcium activity reflects unsigned visuomotor prediction errors.**

693 (**A**) Left: Schematic of the two-photon microscope and virtual reality system. Right: Schematics of the two
694 virtual reality conditions. Top: closed loop condition in which visual flow speed (green) is yoked to
695 locomotion speed (purple). Mismatches consist of 1 s halts in visual flow during locomotion (orange
696 shading). Bottom: open loop condition in which visual flow from the closed loop session is replayed to the
697 mouse uncoupled from locomotion. Playback halts are 1 s halts in visual flow in the open loop condition
698 (gray shading).

699 (**B**) Two-photon calcium imaging of LC axons in the dorsal cortex. Left: NET-Cre mice underwent
700 stereotactic viral vector injections to express axon-targeted GCaMP6s in the LC. 4 weeks later, axons were
701 imaged in two regions of the cortex. Inset shows example two-photon field of view (FoV). Right: Example

ΔF/F traces (black) from three different axons segments in the same FoV, recorded during the closed loop condition. Purple and green traces show locomotion and visual flow speed respectively. Orange shading indicates mismatch events. Gray trace shows pupil diameter.

(**C**) Responses of LC axons to visual flow halt stimuli (left: mismatches, and right: playback halts while the mouse is stationary). Top: Locomotion speed (purple), visual flow speed (green) and absolute error (red; absolute difference between visual flow speed and locomotion speed) each averaged across trials. Middle: Heat map of the average responses of different fields of view (FoVs) sorted according to response magnitude. Bottom: Response averaged across FoVs. Shading indicates SEM.

(**D**) Average responses per FoV to mismatches and playback halts, while the mouse was either stationary or locomoting. Error bars indicate SEM across FoVs. Here and in other panels, n.s.: not significant, *: $p < 0.05$, **: $p < 0.01$, ***: $p < 0.001$. For complete statistical information see **Table S1**.

(**E**) Mean mismatch response of LC axons averaged across FoVs as a function of locomotion speed. Top: Heat map of the average mismatch response, sorted according to locomotion speed (speeds correspond to below plot). Bottom: Mean and SEM (error bars) of the mismatch responses averaged over FoVs as a function of locomotion speed. Only datapoints with at least 10 FoVs in each speed bin are included.

(**F**) Responses of LC axons to visual flow onsets in the open loop condition during locomotion (left) or stationary periods (right), plotted as in panel **C**.

(**G**) Average responses of LC axons to visual flow onsets while the mouse was either locomoting or stationary, plotted as in panel **D**.

(**H**) Responses of LC axons to the different visual flow stimuli in different conditions averaged across FoVs, color coded according to the legend, and plotted as a function of the change in absolute error between locomotion speed and visual flow speed during the stimulus (relative to 1 s prior to stimulus onset). Error bars indicate SEM.

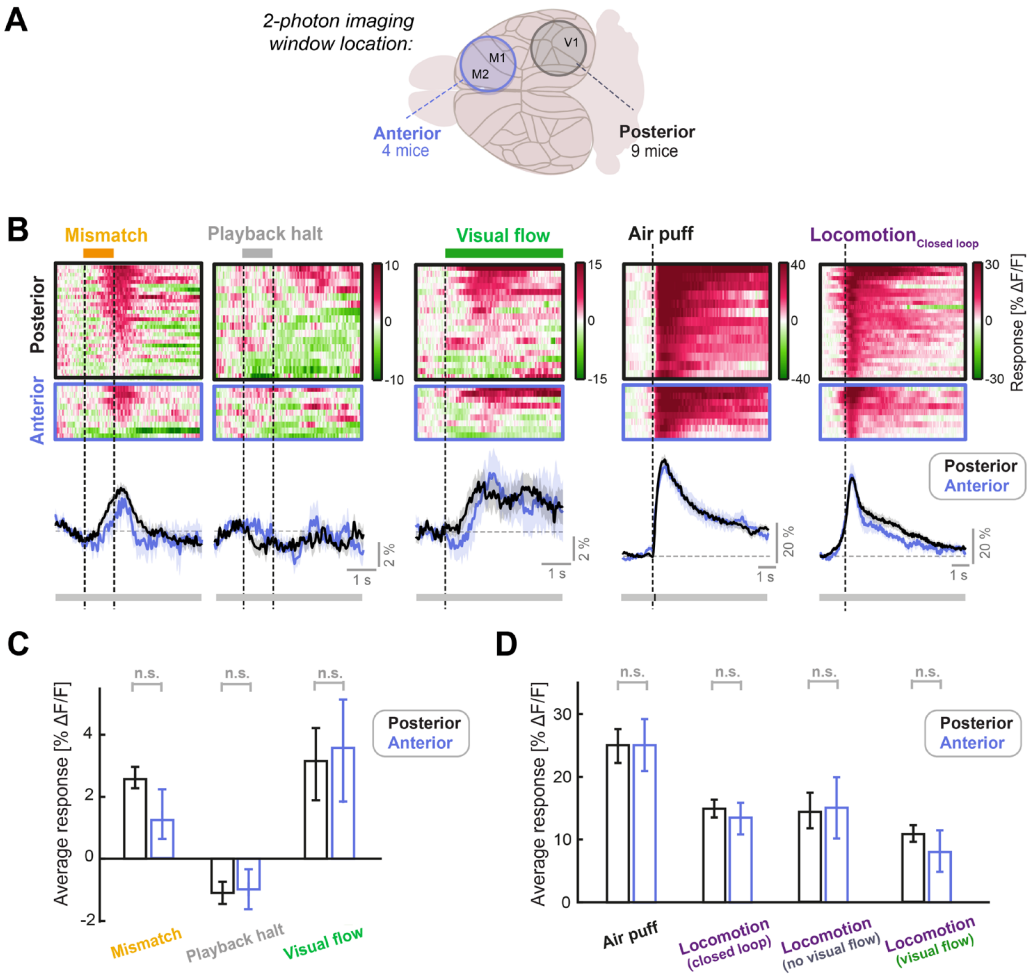

Figure 2. LC axonal responses are similar in sensory (posterior) and motor (anterior) cortical areas.

(**A**) Schematic of the two different locations of the two-photon imaging windows used. Posterior windows were centered on V1 and included surrounding structures, while anterior windows included the primary and secondary motor cortex.

(**B**) Responses of posterior and anterior FoVs to (from left to right): Mismatch, playback halts (stationary), visual flow (stationary), air puff, and locomotion onset in closed loop. Each heatmap is sorted by average response. Color scale is ΔF/F. Traces below heatmaps show average across FoVs, for posterior (black) and anterior (blue) imaging sites. Shading shows SEM. Bar below plot indicates significance of comparison at each time point using an unpaired t-test: grey indicates p>0.01, black indicates p<0.01.

(**C**) Average responses of LC axons to mismatch, playback halt, and visual flow onset averaged across FoVs, compared between posterior and anterior imaging locations. Error bars indicate SEM. Here and in other panels, n.s.: not significant. For complete statistical information see **Table S1**.

(**D**) As in **C**, but for air puff responses (which were infrequently used to evoke locomotion) and locomotion onset responses in various conditions, each averaged in the 3 s window after onset. Note that $\text{locomotion}_{\text{Visual flow}}$ and $\text{locomotion}_{\text{No visual flow}}$ occur in open loop conditions (see also **Figure S2**).

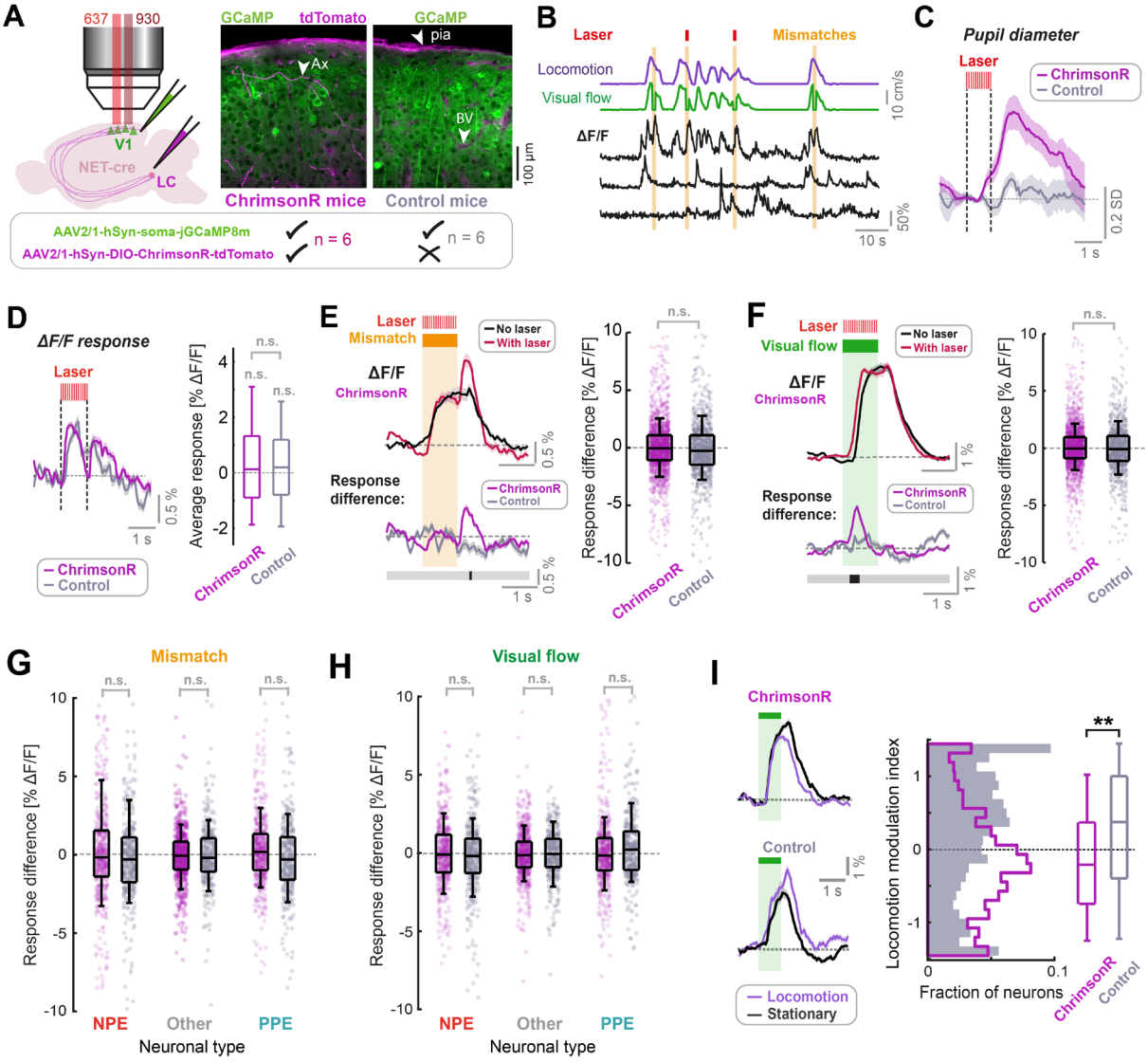

Figure 3. LC axon stimulation has only a small effect on stimulus responses in layer 2/3 of V1.

(**A**) AAV vector injections were used to express ChrimsonR-tdTomato in LC NET-positive neurons, and jGCaMP8m in layer 2/3 neurons of V1. Simultaneous two-photon calcium imaging and optogenetic stimulation with a 637 nm laser would take place in layer 2/3. Injections into the LC were omitted in control mice. Example histology images indicate expression of jGCaMP8m (green) and tdTomato (magenta); note that blood vessels and pia mater (see arrows labelled 'BV' and 'pia' respectively) are also visible in the magenta channel. Arrow labelled 'Ax' indicates an axon.

(**B**) Example ΔF/F traces for three somatic ROIs in layer 2/3 of V1 (black) and the corresponding visual flow speed (green) and locomotion speed (purple) traces. Orange shading indicates visuomotor mismatch events. Red marks indicate concurrent laser stimulation to activate ChrimsonR on a random subset of mismatch trials.

(**C**) Average pupil diameter response to stimulation with the optogenetic laser presented in isolation for ChrimsonR-expressing mice (pink), and control mice (gray). Shading represents SEM.

(**D**) Left: Average population ΔF/F response of layer 2/3 neurons in V1 to the onset of the optogenetic stimulation laser presented in isolation. Right: Boxplots to compare average response (quantified in the window 0.3 to 1.6 s after optogenetic stimulation onset) for the two groups of mice. Here and in other panels, n.s.: not significant. For complete statistical information see **Table S1**.

(**E**) Analysis of mismatch responses of all layer 2/3 neurons. Left: Average population ΔF/F response of layer 2/3 neurons in V1 of ChrimsonR-expressing mice to visuomotor mismatch either with (red) or without (black) concurrent optogenetic laser stimulation. Below plot shows average difference between trials with and without laser stimulation averaged across the population for ChrimsonR-expressing (pink) and control (gray) mice. Bold line below indicates timepoints where control and ChrimsonR-expressing datasets significantly differed (black) or not (gray). Right: Boxplots to compare the difference in average mismatch response between trials with and without optogenetic laser stimulation. Pink points indicate data for each neuron from ChrimsonR-expressing mice, and gray points indicate data from control mice. Note, statistical tests against zero for the effect in ChrimsonR-expressing mice were also insignificant (see **Table S1**).

(**F**) As for **E**, but for responses to 1 s fixed speed visual flow stimuli in open loop conditions.

(**G**) As for boxplots in panel **E**, but for mismatch responses of three different functionally defined neuronal groups: NPE = negative prediction error neurons, with large responses to mismatches, PPE = positive prediction error neurons, with large responses to visual flow, and an intermediate group 'other'. See Methods and **Figure S4** for information on neuronal types. Note, statistical tests against zero for the effect in ChrimsonR-expressing mice were also insignificant (see **Table S1**).

(**H**) As for **G**, but for responses to 1 s fixed speed visual flow stimuli in open loop conditions.

(**I**) Left: Population average responses to visual flow stimuli during stationary periods (black) and during locomotion (purple), for control mice (bottom), and ChrimsonR-expressing mice (top). Shading represents SEM. Note that only trials *without* concurrent optogenetic stimulation are included here. Right: Histograms and boxplots to show distribution of locomotion modulation index for the visual responses recorded in control (gray) and ChrimsonR-expressing mice (pink). Here, **: $p < 0.01$ (see **Table S1**).

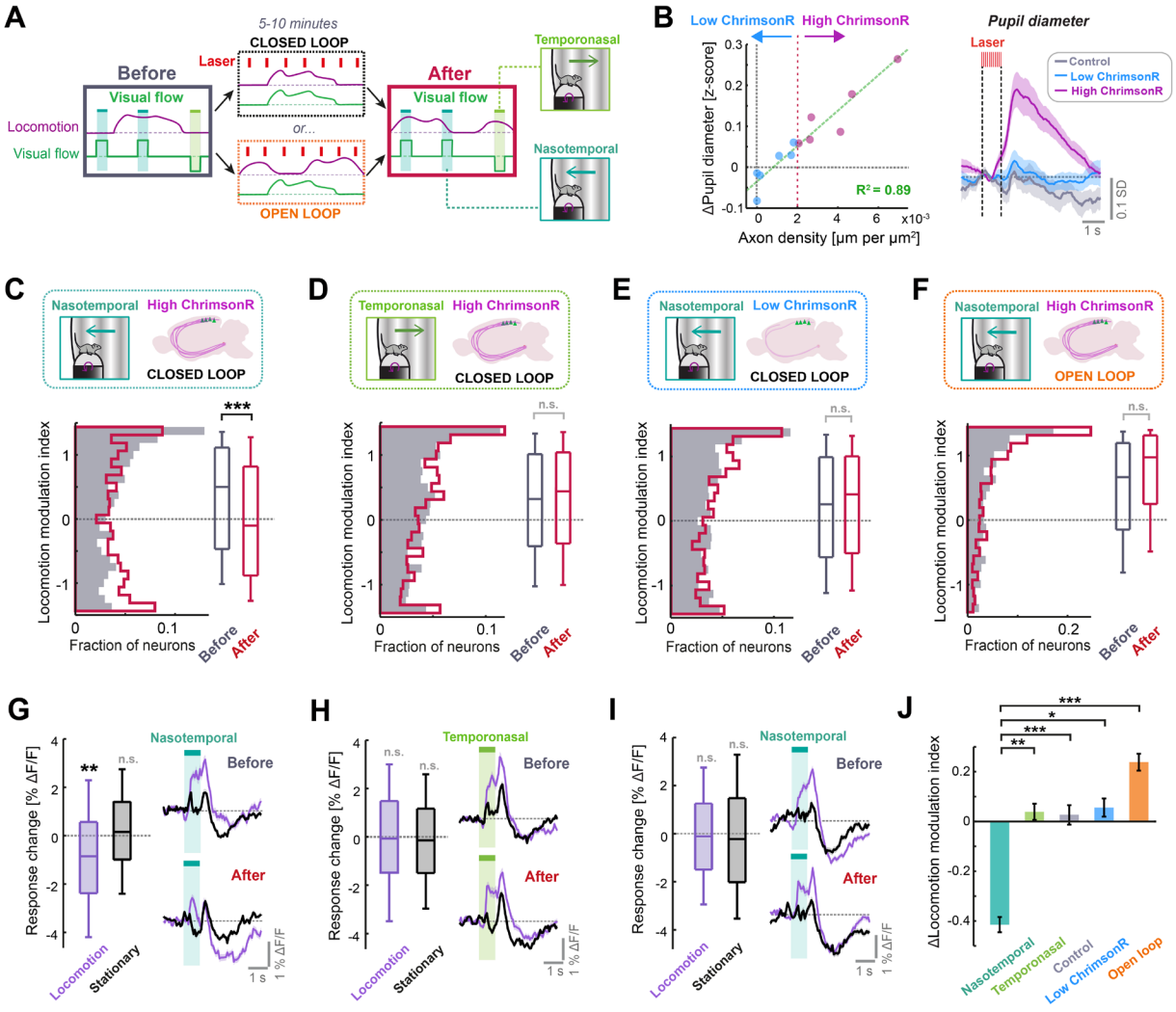

Figure 4. Phasic LC output enhances sensorimotor plasticity in layer 2/3 of V1.

(**A**) Diagram of the experiment used to determine whether LC axon stimulation during different visuomotor coupling conditions can modulate plasticity. Visual responses are compared before and after 5-10 minutes of either closed or open loop conditions, during which LC axons were stimulated every 7 s on average.

(**B**) Left: Scatter plot to show the relationship between density of ChrimsonR-tdTomato labelled axons in V1 (total axon length per unit area of the cortex, analyzed postmortem) and the average evoked pupil dilation during optogenetic stimulation. Green dashed line is a linear regression fit to the data, and red dotted line indicates axon density threshold used to categorize low (blue) and high (pink) ChrimsonR-expressing mice. Right: Average pupil diameter response to stimulation with the optogenetic laser for 6 mice with high ChrimsonR expression in LC axons (pink), 6 mice with low ChrimsonR expression (blue), and 7 control mice that did not receive a vector injection into the LC (black). Shading represents SEM over sessions.

795 (**C**) Analysis of plasticity in nasotemporal visual flow responses in ChrimsonR-expressing mice undergoing
796 optogenetic laser stimulation during closed loop visuomotor experience. Histograms and boxplots show
797 distribution of locomotion modulation indices for the visual responses of layer 2/3 V1 neurons recorded
798 before (dark gray) and after the stimulation period (red). Here and in all other panels: n.s.: not significant,
799 *: $p < 0.05$, **: $p < 0.01$, ***: $p < 0.001$. See **Table S1** for all statistical information.

800 (**D**) As for panel **C**, but for temporonasal visual flow responses.

801 (**E**) As for panel **C**, but for low ChrimsonR-expressing mice.

802 (**F**) As for panel **C**, but for the condition in which optogenetic stimulation occurred during open loop
803 replays of visual flow (i.e., no visuomotor coupling).

804 (**G**) Analysis of plasticity in nasotemporal visual flow responses in high ChrimsonR-expressing mice
805 undergoing optogenetic laser stimulation during the closed loop condition. Left: Boxplots of the change
806 in response to visual flow after optogenetic stimulation for responses recorded during locomotion
807 (purple) and those recorded during stationary periods (black). Right: Average population response to
808 visual flow during locomotion (purple) and during stationary periods (black), before (top) and after
809 (bottom) optogenetic stimulation. Shading indicates SEM.

810 (**H**) As for panel **G**, but for temporonasal visual flow responses.

811 (**I**) As for panel **G**, but for low ChrimsonR-expressing mice.

812 (**J**) Change in locomotion modulation index after optogenetic stimulation, for the four sets of
813 experiments from panels **C** (nasotemporal), **D** (temporonasal), **Figure S5C** (Control), **E** (low ChrimsonR
814 expression), and **F** (open loop) (presented in the respective sequence).

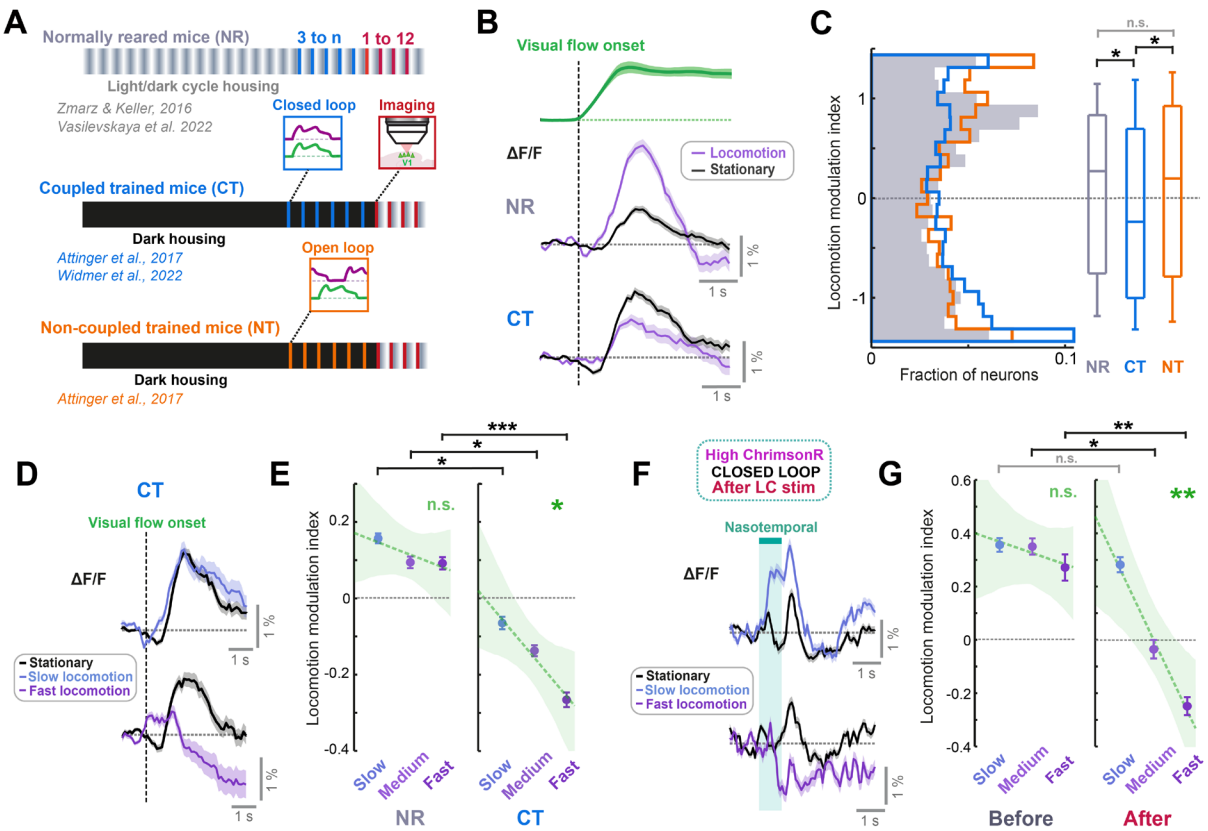

Figure 5. LC axon stimulation over minutes recapitulates the visuomotor plasticity seen over days.

(**A**) Diagram of the three groups of mice reared with different visuomotor experience. Normally reared mice (NR, gray) were raised with a normal light/dark cycle in their cages, with the full diversity of visuomotor coupling in freely moving conditions. Coupled trained mice (CT, blue) were reared in the dark, and their only visuomotor experience prior to imaging was during closed loop conditions in the virtual reality system. Non-coupled trained mice (NT, orange) were reared similar to coupled trained mice, except their only visual experience was during open loop conditions in the virtual reality system.

(**B**) Average population responses of layer 2/3 neurons in V1 to the onset of visual flow during open loop replay sessions. Green shows the average speed profile of the visual flow stimulus, purple shows the average population responses during locomotion, and black shows the average population responses during stationary periods for normally reared (top) and coupled trained (bottom) mice. Shading indicates SEM.

(**C**) Distribution of the locomotion modulation indices of all V1 layer 2/3 neurons for the visual flow onset responses recorded in normally reared (gray), coupled trained (blue), and non-coupled trained (orange) mice. Here and in other panels, n.s.: not significant, *: $p < 0.05$, **: $p < 0.01$, ***: $p < 0.001$. For complete statistical information see **Table S1**.

(**D**) Average population responses of layer 2/3 neurons in V1 in coupled trained mice to the onset of visual flow during stationary periods (black), and during slow (top) and fast (bottom) locomotion (purple). Shading indicates SEM.

835 (**E**) Comparison of locomotion modulation indices averaged across neurons for visual flow onset responses
836 recorded during slow, medium, and fast locomotion speeds, in normally reared (left) and coupled trained
837 (right) mice. Error bars indicate SEM. Green dashed line indicates linear regression fit to the data, and
838 shading indicates the 95% confidence interval of the regression. Green asterisks and 'n.s.' indicate
839 significance of the fit.

840 (**F**) As for panel **D**, but for nasotemporal visual flow responses in high ChrimsonR-expressing mice after LC
841 axon stimulation in closed loop conditions.

842 (**G**) As for panel **E**, but for nasotemporal visual flow responses in high ChrimsonR-expressing mice before
843 (left) and after (right) LC axon stimulation in closed loop visuomotor coupling.

844

845 **SUPPLEMENTARY FIGURES**

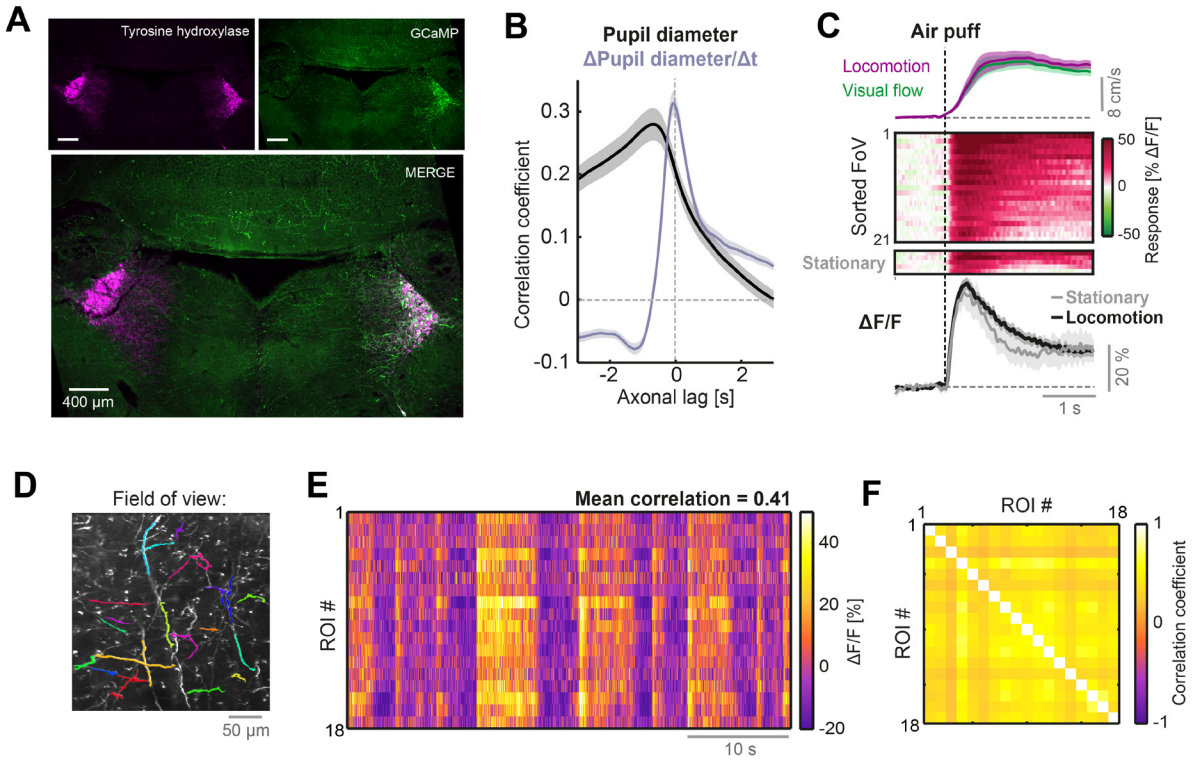

846

847 **Figure S1. Additional information and analyses on two-photon imaging of LC axons. Related to Figure 1.**

848 (**A**) Confocal micrographs showing immunolabelling for tyrosine hydroxylase (magenta) and GCaMP6s
849 (green) in the two LC. GCaMP6s was expressed via stereotactic viral vector injection into only the right
850 LC of NET-Cre mice.

851 (**B**) Cross-correlations between LC axonal ΔF/F and pupil diameter (black) or the time derivative of pupil
852 diameter (gray) averaged across 40 FoVs. Shading indicates SEM. Positive axonal lag values indicate time
853 delays where axonal fluorescence lags relative to pupil diameter or its derivative.

854 (**C**) Responses to air puff stimuli applied to the flank which were infrequently used to evoke locomotion
855 (here during the closed loop condition). Top: Average locomotion speed (purple) and visual flow speed
856 (green) for trials that evoked locomotion. Middle: Heat maps of the average air puff responses of
857 different FoVs sorted according to response magnitude, for trials that evoked locomotion (top heat
858 map) and rare trials that did not evoke locomotion (bottom heat map). Bottom: Response averaged
859 across FoVs for air puff trials that evoked locomotion (black) and those that did not (gray). Shading
860 indicates SEM.

861 (**D**) Example two-photon field of view of LC axons, with 18 regions of interest (ROI) superimposed in
862 different colors.

863 (**E**) Heat map of ΔF/F of the 18 ROIs in panel **D** from a segment of closed loop experience.

864 (**F**) Correlation matrix of the activity of the 18 different ROIs in panels **D** and **E**.

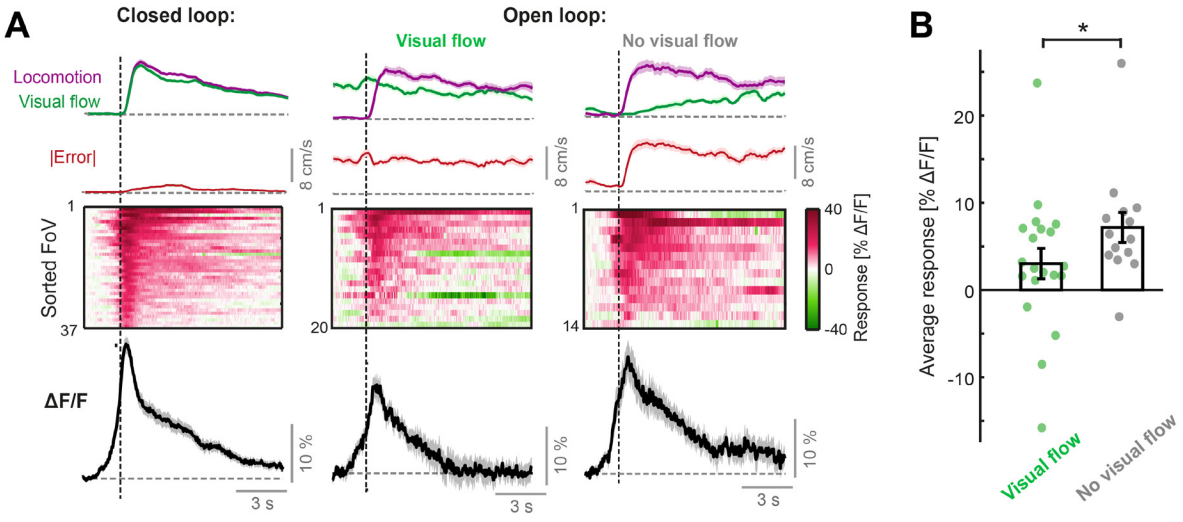

Figure S2. Locomotion onset responses of LC axons. Related to Figure 2.

(**A**) Responses to the onset of locomotion occurring during the closed loop condition (left), during visual flow in the open loop condition (middle), and during no visual flow in the open loop condition (right). Top: Average visual flow speed (green) and locomotion speed (purple) averaged across trials. Note that the window for defining the occurrence of visual flow is in the 2 s window centered on the locomotion onset – therefore the incidence of visual flow increases away from this onset. Red trace shows the absolute error between locomotion speed and visual flow speed averaged across trials (note that, since absolute error is averaged across trials independently, it is *not* equivalent to the absolute difference in averaged locomotion speed and visual flow speed traces plotted above. In addition, note that the minor error occurring in the closed loop condition is due to mismatches). Middle: Heat map of the average responses of different fields of view (FoV) sorted according to response magnitude. Bottom: Response averaged over FoVs. Shading indicates SEM.

(**B**) Comparison of average sustained response of LC axons to locomotion onsets in the open loop condition (quantified in the window 1 to 10 s after locomotion onset), during either visual flow or no visual flow, across FoVs. Each point indicates the average response of an individual FoV. Error bars indicate SEM. *: $p < 0.05$. For statistical information see **Table S1**.

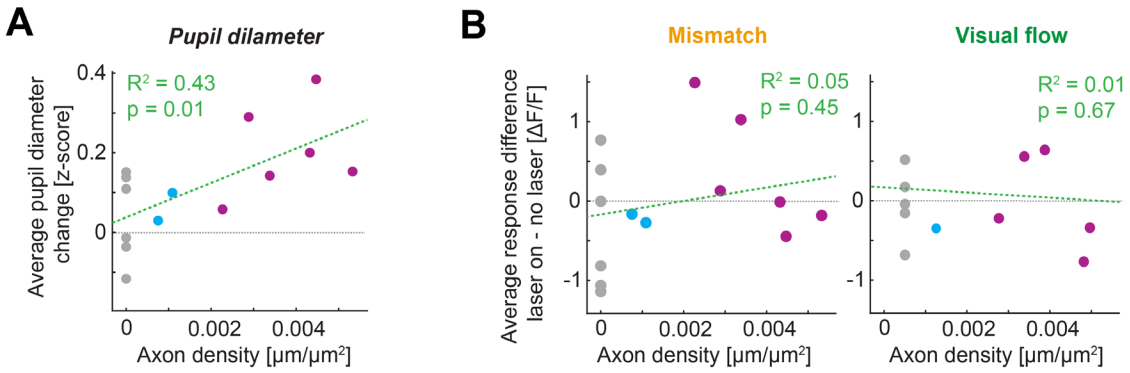

Figure S3. Dependence of laser stimulation effects on ChrimsonR-labelled LC axon density. Related to Figure 3.

(**A**) Laser-evoked change in pupil diameter plotted against ChrimsonR-labelled axon density in V1 (see Methods) for the dataset in **Figure 3**. Pink shows high ChrimsonR-expressing mice, blue shows low ChrimsonR-expressing mice, and gray shows control mice.

(**B**) As in **A**, but for the effect of laser stimulation on average mismatch and visual flow responses, averaged across the population recorded in each mouse.

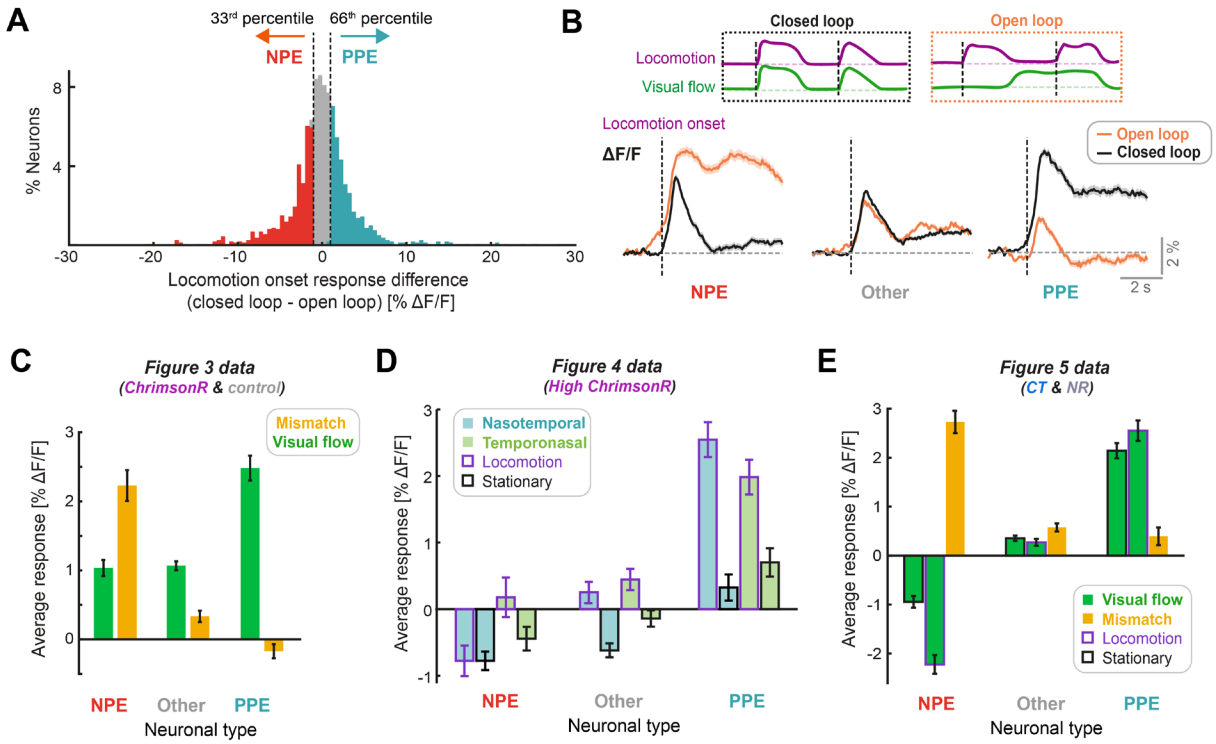

Figure S4. Classification of functional neuronal types in V1 layer 2/3. Related to Figures 3, 4, and 5.

(**A**) Percentage of neurons as a function of the difference in response to locomotion onsets in closed loop conditions and open loop conditions. Neurons with a responses difference below the 33rd percentile (open loop response > closed loop response), were classified as visually suppressed NPE neurons (red), while those with a response difference exceeding the 66th percentile (closed loop response > open loop response), were classified as visually driven PPE neurons (turquoise), as shown. Data for this panel comes from **Figure 3** dataset.

(**B**) Top: Diagram of visual flow and locomotion speed traces to indicate closed loop and open loop locomotion onsets (black dashed lines). Bottom: Responses to locomotion onset during closed loop and open loop, averaged across neurons classified as NPE, PPE, and the intermediate group (Other). Shading indicates SEM. Data for this panel comes from **Figure 3** dataset.

(**C**) Bar graph to show visual flow and visuomotor mismatch responses, averaged across neurons, compared for the three functional neuron types: NPE, Other, and PPE neurons. Error bars indicate SEM. Data for this panel comes from **Figure 3** dataset.

(**D**) Bar graph to show nasotemporal and temporonasal visual flow responses (split further into occurring during locomotion or stationary periods), averaged across neurons, compared for the three functional neuron types: NPE, Other, and PPE neurons. Error bars indicate SEM. Data for this panel comes from **Figure 4** dataset (High ChrimsonR only). Mismatch data was not acquired for this dataset.

(**E**) Bar graph to show visual flow onset and visuomotor mismatch responses, averaged across neurons, compared between NPE, Other, and PPE cell classes. Error bars indicate SEM. Data for this panel comes from **Figure 5** datasets (coupled trained and normally reared mice).

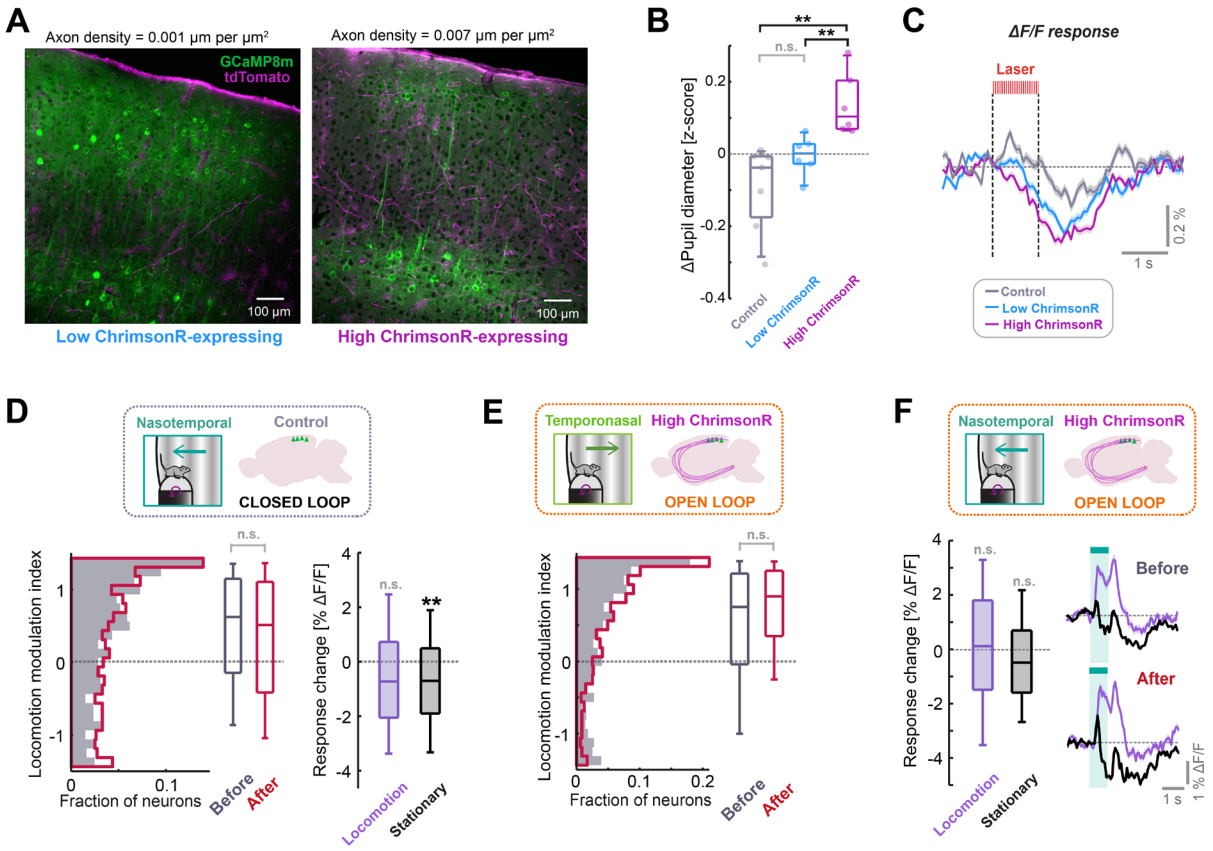

Figure S5. Additional information and analyses on optogenetic stimulation of LC axons to drive plasticity. Related to Figure 4.

(**A**) Two example confocal microscopy images from V1 showing jGCaMP8m expression (green) and tdTomato expression (magenta), indicating labelled LC axons. The right image is from an animal classified as high ChrimsonR-expressing, based on labelled axon density, and left image is from an animal classified as low ChrimsonR-expressing.

(**B**) Comparison of average pupil diameter response (quantified in the window 1.3 to 4.7 s after optogenetic stimulation onset) for control, low ChrimsonR-expressing and high ChrimsonR-expressing mice. Here and in other panels, n.s.: $p > 0.05$, *: $p < 0.05$, **: $p < 0.01$, ***: $p < 0.001$. For complete statistical information see **Table S1**.

(**C**) Average population ΔF/F response of layer 2/3 neurons in V1 to the onset of the optogenetic stimulation laser. Shading indicates SEM. Note that optogenetic laser power was lowered compared to the value used in **Figure 3**, and the positive response seen in **Figure 3D** is no longer evident.

(**D**) Analysis of plasticity in nasotemporal visual flow responses in control mice which underwent optogenetic laser stimulation during the closed loop condition. Left: Distribution of locomotion modulation index for the visual responses recorded before (dark gray) and after the stimulation period (red). Right: Change in ΔF/F response to visual flow after optogenetic stimulation for responses recorded during locomotion (purple) and during stationary periods (black).

932 (**E**) As for panel **D**, but for temporonasal visual flow responses recorded in high ChrimsonR-expressing
933 mice, where optogenetic stimulation occurred during open loop replays of visual flow (i.e., uncoupled
934 from locomotion).

935 (**F**) Analysis of plasticity in nasotemporal visual flow responses for high ChrimsonR-expressing mice which
936 underwent optogenetic laser stimulation during open loop replays of visual flow (i.e., uncoupled from
937 locomotion). Boxplot shows the change in ΔF/F response to visual flow after optogenetic stimulation for
938 responses recorded during locomotion (purple) and during stationary periods (black). Traces show
939 average population response to visual flow during locomotion (purple) and during stationary periods
940 (black), before (top) and after (below) optogenetic stimulation. Shading indicates SEM.

941

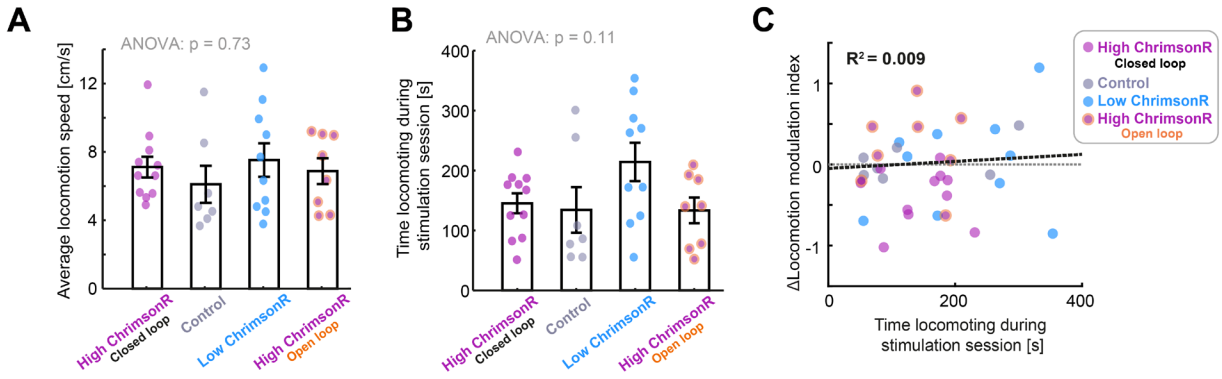

Figure S6. Differences in locomotion during stimulation cannot explain differences in the change of locomotion modulation index between groups. Related to Figure 4.

(**A**) Average locomotion speed (excluding stationary periods) for: High ChrimsonR-expressing mice during closed loop stimulation, Control mice during closed loop stimulation, low ChrimsonR-expressing mice during closed loop stimulation, and high ChrimsonR-expressing mice during open loop stimulation. Points show data for each imaging session.

(**B**) As for panel **A**, but for the time spent engaged in locomotion during the stimulation period.

(**C**) Change in locomotion modulation index after optogenetic stimulation plotted against the time spent engaged in locomotion during the laser stimulation period of the imaging session. Each point shows the averages for a single imaging session.

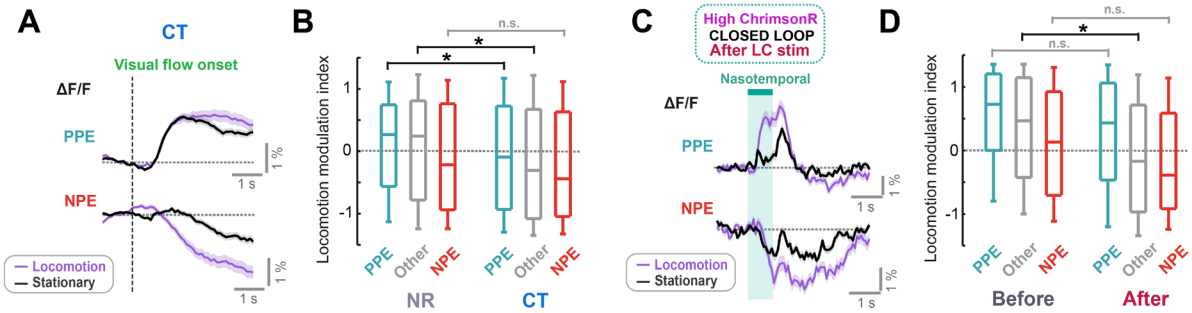

954

955 **Figure S7. Comparison of locomotion modulation index across different functional neuronal types in**
956 **layer 2/3 V1. Related to Figure 5.**

957 (**A**) Average population responses of layer 2/3 neurons in V1 in coupled trained mice to the onset of visual
958 flow during stationary periods (black), and during locomotion (purple) for visually driven positive
959 prediction error neurons (PPE, top) and visually suppressed negative prediction error neurons (NPE,
960 bottom). Shading indicates SEM.

961 (**B**) Comparison of locomotion modulation index for visual flow onset responses of positive (turquoise),
962 negative (orange) prediction error neurons, and an intermediate population of neurons (gray), recorded
963 in normally reared (left) and coupled trained (right) mice. For information on functional neuron types, see
964 **Figure S4**. Here and in other panels, n.s.: $p > 0.05$, *: $p < 0.05$, **: $p < 0.01$, ***: $p < 0.001$. For complete
965 statistical information see **Table S1**.

966 (**C**) As for panel **A**, but for nasotemporal visual flow responses in high ChrimsonR-expressing mice after LC
967 axon stimulation in closed loop conditions.

968 (**D**) As for panel **B**, but for nasotemporal visual flow responses in high ChrimsonR-expressing mice before
969 (left) and after (right) LC axon stimulation in closed loop conditions.

970 **TABLES**

971 **Table S1.** All statistical information.

Figure panel	Comparison	Value compared	Mean 1 *(delta shown for paired tests)*	SD 1	Mean 2 *(n/a for paired tests)*	SD 2	Test type	P-value	N (ROIs)	N (Sites)	N (Mice)
1D	Mean response *vs* zero	Playback halt response (stationary) [% ΔF/F]	-1.07	1.71	n/a	n/a	Paired t-test	**0.0045**	n/a	25	10
	Mismatch *vs* Playback halt (locomotion)	Mean response [% ΔF/F]	2.24	2.30	0.64	3.51	Rank-sum	**0.0497**	n/a	40,24	13,10
	Playback halt locomotion *vs* stationary	Mean response [% ΔF/F]	0.64	3.51	-1.07	1.71	Rank-sum	**0.0080**	n/a	24,25	10,10
	Mean response *vs* zero	Playback halt response (locomotion) [% ΔF/F]	0.64	3.51	n/a	n/a	Paired t-test	0.3841	n/a	24	10
	Mean response *vs* zero	Mismatch response [% ΔF/F]	2.24	2.30	n/a	n/a	Paired t-test	**$< 10^{-5}$**	n/a	40	13
	Mismatch *vs* Playback halt (stationary)	Mean response [% ΔF/F]	2.24	2.30	-1.07	1.71	Unpaired t-test	**$< 10^{-5}$**	n/a	40,25	13,10
1G	Mean response *vs* zero	Visual flow response (stationary) [% ΔF/F]	3.19	5.31	n/a	n/a	Signed-rank test	**0.0031**	n/a	28	11
	Locomotion *vs* stationary	Mean visual response [% ΔF/F]	-0.55	4.24	3.19	5.31	Rank-sum	**0.0133**	n/a	21,28	11,11
	Mean response *vs* zero	Visual flow response (locomoting) [% ΔF/F]	-0.55	4.24	n/a	n/a	Paired t-test	0.5598	n/a	21	11
2B	Posterior *vs* Anterior	Mismatch response [% ΔF/F]	2.56	2.03	1.18	2.94	Unpaired t-test	0.1127	n/a	31, 9	9,4
	Posterior *vs* Anterior	Playback halt response (stationary) [% ΔF/F]	-1.11	1.56	-1.00	2.05	Unpaired t-test	0.8801	n/a	16, 9	6, 4
	Posterior *vs* Anterior	Visual flow response (stationary) [% ΔF/F]	2.99	5.49	3.60	5.20	Unpaired t-test	0.7855	n/a	19, 9	7, 4
2C	Posterior *vs* Anterior	Locomotion response (visual flow) [% ΔF/F]	10.85	5.89	8.12	8.46	Rank-sum	0.3025	n/a	14, 6	6, 3
	Posterior *vs* Anterior	Locomotion response (closed loop) [% ΔF/F]	14.99	7.07	13.33	7.86	Rank-sum	0.4257	n/a	28, 9	9,4
	Posterior *vs* Anterior	Locomotion response (no visual flow) [% ΔF/F]	14.42	8.05	14.96	11.93	Unpaired t-test	0.9202	n/a	8, 6	6, 3
	Posterior *vs* Anterior	Air puff response [% ΔF/F]	24.73	10.03	24.48	11.23	Unpaired t-test	0.9581	n/a	13, 8	6,4
3D	Mean response *vs* zero	ChrimsonR, laser response [% ΔF/F]	0.40	2.69	n/a	n/a	Bootstrap	0.0775	1985	15	6
	Mean response *vs* zero	Control, laser response [% ΔF/F]	0.30	2.24	n/a	n/a	Bootstrap	0.1785	1026	10	6
	Control *vs* ChrimsonR	Laser response [% ΔF/F]	0.30	2.24	0.40	2.69	Bootstrap	0.3929	1026, 1985	10,15	6,6
3E	Control *vs* ChrimsonR	Mismatch response difference [% ΔF/F]	-0.26	3.39	0.05	2.86	Bootstrap	0.2244	1053, 1911	10,14	6,6
	Optogenetic stimulation *vs* no stimulation	ChrimsonR, mismatch response [% ΔF/F]	0.05	2.86	n/a	n/a	Bootstrap	0.4189	1911	14	6
3F	Control *vs* ChrimsonR	Visual flow response difference [% ΔF/F]	-0.04	2.43	0.06	2.43	Bootstrap	0.3852	1053, 2233	10,16	6,6
	Optogenetic stimulation *vs* no stimulation	ChrimsonR, visual flow response [% ΔF/F]	0.06	2.34	n/a	n/a	Bootstrap	0.3869	2233	16	6
3G	Control *vs* ChrimsonR	PPE, mismatch response difference [% ΔF/F]	-0.20	2.97	0.25	2.93	Bootstrap	0.1432	369, 541	10,12	6,6
	Control *vs* ChrimsonR	NPE, mismatch response difference [% ΔF/F]	-0.47	4.41	0.21	3.81	Bootstrap	0.1771	382, 525	10,12	6,6
	Optogenetic stimulation *vs* no stimulation	ChrimsonR PPE, mismatch response [% ΔF/F]	0.25	2.93	n/a	n/a	Bootstrap	0.2177	541	12	6
	Optogenetic stimulation *vs* no stimulation	ChrimsonR NPE, mismatch response [% ΔF/F]	0.21	3.81	n/a	n/a	Bootstrap	0.3433	525	12	6
	Control *vs* ChrimsonR	Other, mismatch response difference [% ΔF/F]	-0.02	2.22	-0.08	1.92	Bootstrap	0.5335	275, 526	10,12	6,6
	Optogenetic stimulation *vs* no stimulation	ChrimsonR Other, mismatch response [% ΔF/F]	-0.08	1.92	n/a	n/a	Bootstrap	0.6313	526	12	6

3H	Control *vs* ChrimsonR	PPE, visual flow response difference [% ΔF/F]	0.33	2.86	0.09	3.19	Bootstrap	0.7156	369, 541	10,12	6,6
	Control *vs* ChrimsonR	NPE, visual flow response difference [% ΔF/F]	-0.20	2.18	-0.19	2.31	Bootstrap	0.4995	382, 525	10,12	6,6
	Optogenetic stimulation *vs* no stimulation	ChrimsonR PPE, visual flow response [% ΔF/F]	0.09	3.19	n/a	n/a	Bootstrap	0.3983	541	12	6
	Control *vs* ChrimsonR	Other, visual flow response difference [% ΔF/F]	-0.13	1.79	-0.08	1.49	Bootstrap	0.4584	275, 526	10,12	6,6
	Optogenetic stimulation *vs* no stimulation	ChrimsonR Other, visual flow response [% ΔF/F]	-0.08	1.49	n/a	n/a	Bootstrap	0.6316	526	12	6
	Optogenetic stimulation *vs* no stimulation	ChrimsonR NPE, visual flow response [% ΔF/F]	-0.19	2.31	n/a	n/a	Bootstrap	0.7564	525	12	6
3I	Control *vs* ChrimsonR	Locomotion modulation index	0.22	0.84	-0.15	0.72	Bootstrap	**0.0012**	816, 1687	8,12	5,6
4C	Before *vs* After	Locomotion modulation index	-0.42	1.00	n/a	n/a	Bootstrap	**$< 10^{-5}$**	1066	11	5
4D	Before *vs* After	Locomotion modulation index	0.04	1.08	n/a	n/a	Bootstrap	0.6271	1111	11	5
4E	Before *vs* After	Locomotion modulation index	0.06	1.25	n/a	n/a	Bootstrap	0.5922	1140	10	5
4F	Before *vs* After	Locomotion modulation index	0.24	0.98	n/a	n/a	Bootstrap	0.9278	832	8	4
4G	Before *vs* After	Visual response (locomotion) [% ΔF/F]	-0.88	3.54	n/a	n/a	Bootstrap	**0.0013**	1066	11	5
	Before *vs* After	Visual response (stationary) [% ΔF/F]	0.17	2.36	n/a	n/a	Bootstrap	0.6929	1276	13	5
4H	Before *vs* After	Visual response (stationary) [% ΔF/F]	-0.17	2.61	n/a	n/a	Bootstrap	0.2579	1276	13	5
	Before *vs* After	Visual response (locomotion) [% ΔF/F]	-0.06	3.34	n/a	n/a	Bootstrap	0.4043	1111	11	5
4I	Before *vs* After	Visual response (stationary) [% ΔF/F]	-0.28	2.97	n/a	n/a	Bootstrap	0.2404	1140	10	5
	Before *vs* After	Visual response (locomotion) [% ΔF/F]	-0.08	2.61	n/a	n/a	Bootstrap	0.3878	1344	12	5
4J	Open loop *vs* Nasotemporal	Δ locomotion modulation index	0.24	0.98	-0.42	1.00	Bootstrap	**0.0007**	832, 1066	8, 11	4, 5
	Low expression *vs* Nasotemporal	Δ locomotion modulation index	0.06	1.25	-0.42	1.00	Bootstrap	**0.0264**	1140, 1066	10, 11	5, 5
	Control *vs* Nasotemporal	Δ locomotion modulation index	0.03	1.01	-0.42	1.00	Bootstrap	**0.0002**	646, 1066	7, 11	3, 5
	Temporonasal *vs* Nasotemporal	Δ locomotion modulation index	0.04	1.08	-0.42	1.00	Bootstrap	**0.0014**	1111, 1066	11, 11	5, 5
5C	CT *vs* NR	Locomotion modulation index	-0.14	0.92	0.08	0.87	Bootstrap	**0.0164**	4247, 4383	24,26	19,23
	NT *vs* CT	Locomotion modulation index	0.08	0.92	-0.14	0.92	Bootstrap	**0.0308**	1969, 4247	12, 24	8,19
	NR *vs* NT	Locomotion modulation index	0.08	0.87	0.08	0.92	Bootstrap	0.5093	4383, 1969	26,12	23,8
5E	NR *vs* CT	Locomotion modulation index, fast locomotion	0.09	0.88	-0.27	0.90	Bootstrap	**0.0008**	3042, 2298	16,15	15,12
	NR *vs* CT	Locomotion modulation index, slow locomotion	0.16	0.87	-0.07	0.88	Bootstrap	**0.0118**	4669, 2907	31,18	29,16
	NR *vs* CT	Locomotion modulation index, medium locomotion	0.10	0.89	-0.14	0.94	Bootstrap	**0.0178**	4098, 3481	25,21	22,17
5G	Before *vs* After	Locomotion modulation index, fast locomotion	0.27	0.97	-0.25	0.92	Bootstrap	**0.0024**	389, 755	4,7	3,4
	Before *vs* After	Locomotion modulation index, medium locomotion	0.35	0.90	-0.03	0.93	Bootstrap	**0.0429**	872, 723	9,8	5,5
	Before *vs* After	Locomotion modulation index, slow locomotion	0.36	0.85	0.28	0.91	Bootstrap	0.3475	1123, 1043	12,11	5,5
S2B	With *vs* without visual flow	Locomotion onset response (open loop) [% ΔF/F]	3.03	7.82	7.17	6.45	Rank-sum	**0.0442**	n/a	20,14	9,9
S5B	Control *vs* High expression	Pupil diameter response [z-score]	-0.09	0.12	0.14	0.09	Unpaired t-test	**0.0024**	n/a	n/a	7,6
	High expression *vs* Low expression	Pupil diameter response [z-score]	0.14	0.09	0.00	0.05	Unpaired t-test	**0.0071**	n/a	n/a	6,6
	Low expression *vs* Control	Pupil response [z-score]	0.00	0.05	-0.09	0.12	Unpaired T-test	0.1242	n/a	n/a	6,7
S5D	Before *vs* After	Visual response (stationary) [% ΔF/F]	-0.70	3.12	n/a	n/a	Bootstrap	**0.003**	793	8	4
	Before *vs* After	Visual response (locomotion) [% ΔF/F]	-0.57	3.83	n/a	n/a	Bootstrap	0.0534	1163	12	5
	Before *vs* After	Locomotion modulation index	0.03	1.01	n/a	n/a	Bootstrap	0.5909	646	7	3

S5E	Before *vs* After	Locomotion modulation index	0.17	1.02	n/a	n/a	Bootstrap	0.8755	718	7	4
S5F	Before *vs* After	Visual response (stationary) [% ΔF/F]	-0.44	2.31	n/a	n/a	Bootstrap	0.1088	832	8	4
	Before *vs* After	Visual response (locomotion) [% ΔF/F]	-0.07	3.47	n/a	n/a	Bootstrap	0.4273	832	8	4
S7B	NR *vs* CT	Locomotion modulation index, other	0.07	0.89	-0.18	0.94	Bootstrap	**0.0341**	1276, 1384	23,24	22,19
	NR *vs* CT	Locomotion modulation index, NPE	-0.10	0.90	-0.22	0.91	Bootstrap	0.1196	1510, 1108	23,24	22,19
	NR *vs* CT	Locomotion modulation index, PPE	0.11	0.81	-0.07	0.90	Bootstrap	**0.0436**	986, 1755	23,24	22,19
S7D	Before *vs* After	Locomotion modulation index, other	0.33	0.90	-0.13	0.93	Bootstrap	**0.0239**	378, 408	13,13	5,5
	Before *vs* After	Locomotion modulation index, NPE	0.12	0.88	-0.18	0.87	Bootstrap	0.0706	401, 418	13,13	5,5
	Before *vs* After	Locomotion modulation index, PPE	0.51	0.80	0.25	0.92	Bootstrap	0.1006	372, 365	13,13	5,5

REFERENCES

Aston-Jones, G., Bloom, F.E., 1981. Activity of norepinephrine-containing locus coeruleus neurons in behaving rats anticipates fluctuations in the sleep-waking cycle. J. Neurosci. 1, 876–886. https://doi.org/10.1523/JNEUROSCI.01-08-00876.1981

Attinger, A., Wang, B., Keller, G.B., 2017. Visuomotor Coupling Shapes the Functional Development of Mouse Visual Cortex. Cell 169, 1291-1302.e14. https://doi.org/10.1016/j.cell.2017.05.023

Basu, A., Yang, J.-H., Yu, A., Glaeser-Khan, S., Feng, J., Krystal, J.H., Li, Y., Kaye, A.P., 2022. Prefrontal norepinephrine represents a threat prediction error under uncertainty (preprint). Neuroscience. https://doi.org/10.1101/2022.10.13.511463

Bennett, C., Arroyo, S., Hestrin, S., 2013. Subthreshold mechanisms underlying state-dependent modulation of visual responses. Neuron 80, 350–357. https://doi.org/10.1016/j.neuron.2013.08.007

Bouret, S., Sara, S.J., 2004. Reward expectation, orientation of attention and locus coeruleus-medial frontal cortex interplay during learning. Eur. J. Neurosci. 20, 791–802. https://doi.org/10.1111/j.1460-9568.2004.03526.x

Breton-Provencher, V., Drummond, G.T., Feng, J., Li, Y., Sur, M., 2022. Spatiotemporal dynamics of noradrenaline during learned behaviour. Nature 1–7. https://doi.org/10.1038/s41586-022-04782-2

Chandler, D.J., Jensen, P., McCall, J.G., Pickering, A.E., Schwarz, L.A., Totah, N.K., 2019. Redefining Noradrenergic Neuromodulation of Behavior: Impacts of a Modular Locus Coeruleus Architecture. J. Neurosci. 39, 8239–8249. https://doi.org/10.1523/JNEUROSCI.1164-19.2019

Choi, S.-Y., Chang, J., Jiang, B., Seol, G.-H., Min, S.-S., Han, J.-S., Shin, H.-S., Gallagher, M., Kirkwood, A., 2005. Multiple receptors coupled to phospholipase C gate long-term depression in visual cortex. J. Neurosci. Off. J. Soc. Neurosci. 25, 11433–11443. https://doi.org/10.1523/JNEUROSCI.4084-05.2005

Cox, J., Witten, I.B., 2019. Striatal circuits for reward learning and decision-making. Nat. Rev. Neurosci. 20, 482–494. https://doi.org/10.1038/s41583-019-0189-2

Danskin, B., Denman, D., Valley, M., Ollerenshaw, D., Williams, D., Groblewski, P., Reid, C., Olsen, S., Waters, J., 2015. Optogenetics in Mice Performing a Visual Discrimination Task: Measurement and Suppression of Retinal Activation and the Resulting Behavioral Artifact. PLOS ONE 10, e0144760. https://doi.org/10.1371/journal.pone.0144760

Deitcher, Y., Leibner, Y., Kutzkel, S., Zylbermann, N., London, M., 2019. Nonlinear relationship between multimodal adrenergic responses and local dendritic activity in primary sensory cortices. https://doi.org/10.1101/814657

Dombeck, D.A., Khabbaz, A.N., Collman, F., Adelman, T.L., Tank, D.W., 2007. Imaging Large-Scale Neural Activity with Cellular Resolution in Awake, Mobile Mice. Neuron 56, 43–57. https://doi.org/10.1016/j.neuron.2007.08.003

Dvorkin, R., Shea, S.D., 2022. Precise and Pervasive Phasic Bursting in Locus Coeruleus during Maternal Behavior in Mice. J. Neurosci. Off. J. Soc. Neurosci. 42, 2986–2999. https://doi.org/10.1523/JNEUROSCI.0938-21.2022

Eliades, S.J., Wang, X., 2008. Neural substrates of vocalization feedback monitoring in primate auditory cortex. Nature 453, 1102–1106. https://doi.org/10.1038/nature06910

Erisken, S., Vaiceliunaite, A., Jurjut, O., Fiorini, M., Katzner, S., Busse, L., 2014. Effects of Locomotion Extend throughout the Mouse Early Visual System. Curr. Biol. 24, 2899–2907. https://doi.org/10.1016/j.cub.2014.10.045

Ferguson, K.A., Cardin, J.A., 2020. Mechanisms underlying gain modulation in the cortex. Nat. Rev. Neurosci. 21, 80–92. https://doi.org/10.1038/s41583-019-0253-y

Flagel, S.B., Clark, J.J., Robinson, T.E., Mayo, L., Czuj, A., Willuhn, I., Akers, C.A., Clinton, S.M., Phillips, P.E.M., Akil, H., 2011. A selective role for dopamine in stimulus–reward learning. Nature 469, 53–57. https://doi.org/10.1038/nature09588

Foote, S.L., Aston-Jones, G., Bloom, F.E., 1980. Impulse activity of locus coeruleus neurons in awake rats and monkeys is a function of sensory stimulation and arousal. Proc. Natl. Acad. Sci. U. S. A. 77, 3033–3037.

Glennon, E., Carcea, I., Martins, A.R.O., Multani, J., Shehu, I., Svirsky, M.A., Froemke, R.C., 2019. Locus Coeruleus Activation Accelerates Perceptual Learning. Brain Res. 1709, 39–49. https://doi.org/10.1016/j.brainres.2018.05.048

Glennon, E., Valtcheva, S., Zhu, A., Wadghiri, Y.Z., Svirsky, M.A., Froemke, R.C., 2023. Locus coeruleus activity improves cochlear implant performance. Nature 613, 317–323. https://doi.org/10.1038/s41586-022-05554-8

Greenstreet, F., Vergara, H.M., Pati, S., Schwarz, L., Wisdom, M., Marbach, F., Johansson, Y., Rollik, L., Moskovitz, T., Clopath, C.M., Stephenson-Jones, M., 2022. Action prediction error: a value-free dopaminergic teaching signal that drives stable learning. https://doi.org/10.1101/2022.09.12.507572

He, K., Huertas, M., Hong, S.Z., Tie, X., Hell, J.W., Shouval, H., Kirkwood, A., 2015. Distinct Eligibility Traces for LTP and LTD in Cortical Synapses. Neuron 88, 528–538. https://doi.org/10.1016/j.neuron.2015.09.037

Heindorf, M., Keller, G.B., 2022. Reduction of layer 5 mediated long-range cortical communication by antipsychotic drugs. https://doi.org/10.1101/2022.01.31.478462

Hervé-Minvielle, A., Sara, S.J., 1995. Rapid habituation of auditory responses of locus coeruleus cells in anaesthetized and awake rats. Neuroreport 6, 1363–1368. https://doi.org/10.1097/00001756-199507100-00001

Hong, S.Z., Mesik, L., Grossman, C.D., Cohen, J.Y., Lee, B., Severin, D., Lee, H.-K., Hell, J.W., Kirkwood, A., 2022. Norepinephrine potentiates and serotonin depresses visual cortical responses by transforming eligibility traces. Nat. Commun. 13, 3202. https://doi.org/10.1038/s41467-022-30827-1

Jordan, R., Keller, G.B., 2020. Opposing Influence of Top-down and Bottom-up Input on Excitatory Layer 2/3 Neurons in Mouse Primary Visual Cortex. Neuron. https://doi.org/10.1016/j.neuron.2020.09.024

Kasamatsu, T., Pettigrew, J.D., 1976. Depletion of brain catecholamines: failure of ocular dominance shift after monocular occlusion in kittens. Science 194, 206–209. https://doi.org/10.1126/science.959850

Kasamatsu, T., Watabe, K., Heggelund, P., Schöller, E., 1985. Plasticity in cat visual cortex restored by electrical stimulation of the locus coeruleus. Neurosci. Res. 2, 365–386. https://doi.org/10.1016/0168-0102(85)90047-1

Kebschull, J.M., Garcia da Silva, P., Reid, A.P., Peikon, I.D., Albeanu, D.F., Zador, A.M., 2016. High-Throughput Mapping of Single-Neuron Projections by Sequencing of Barcoded RNA. Neuron 91, 975–987. https://doi.org/10.1016/j.neuron.2016.07.036

Keller, G.B., Bonhoeffer, T., Hübener, M., 2012. Sensorimotor mismatch signals in primary visual cortex of the behaving mouse. Neuron 74, 809–815. https://doi.org/10.1016/j.neuron.2012.03.040

Keller, G.B., Mrsic-Flogel, T.D., 2018. Predictive Processing: A Canonical Cortical Computation. Neuron 100, 424–435. https://doi.org/10.1016/j.neuron.2018.10.003

1064 Kim, H.R., Malik, A.N., Mikhael, J.G., Bech, P., Tsutsui-Kimura, I., Sun, F., Zhang, Y., Li, Y., Watabe-Uchida,
1065 M., Gershman, S.J., Uchida, N., 2020. A Unified Framework for Dopamine Signals across
1066 Timescales. Cell 183, 1600-1616.e25. https://doi.org/10.1016/j.cell.2020.11.013
1067 Leinweber, M., Ward, D.R., Sobczak, J.M., Attinger, A., Keller, G.B., 2017. A Sensorimotor Circuit in
1068 Mouse Cortex for Visual Flow Predictions. Neuron 95, 1420-1432.e5.
1069 https://doi.org/10.1016/j.neuron.2017.08.036
1070 Liu, Y., Rodenkirch, C., Moskowitz, N., Schriver, B., Wang, Q., 2017. Dynamic Lateralization of Pupil
1071 Dilation Evoked by Locus Coeruleus Activation Results from Sympathetic not Parasympathetic
1072 Contributions. Cell Rep. 20, 3099–3112. https://doi.org/10.1016/j.celrep.2017.08.094
1073 Martins, A.R.O., Froemke, R.C., 2015. Coordinated forms of noradrenergic plasticity in the locus
1074 coeruleus and primary auditory cortex. Nat. Neurosci. 18, 1483–1492.
1075 https://doi.org/10.1038/nn.4090
1076 McKinney, A., Hu, M., Hoskins, A., Mohammadyar, A., Naeem, N., Jing, J., Patel, S.S., Sheth, B.R., Jiang,
1077 X., 2022. Cellular and Circuit Organization of the Locus Coeruleus of Adult Mice.
1078 https://doi.org/10.1101/2022.03.01.481656
1079 Meijering, E., Jacob, M., Sarria, J.-C.F., Steiner, P., Hirling, H., Unser, M., 2004. Design and validation of a
1080 tool for neurite tracing and analysis in fluorescence microscopy images. Cytom. Part J. Int. Soc.
1081 Anal. Cytol. 58, 167–176. https://doi.org/10.1002/cyto.a.20022
1082 Mu, Y., Bennett, D.V., Rubinov, M., Narayan, S., Yang, C.-T., Tanimoto, M., Mensh, B.D., Looger, L.L.,
1083 Ahrens, M.B., 2019. Glia Accumulate Evidence that Actions Are Futile and Suppress Unsuccessful
1084 Behavior. Cell 178, 27-43.e19. https://doi.org/10.1016/j.cell.2019.05.050
1085 Mukamel, E.A., Nimmerjahn, A., Schnitzer, M.J., 2009. Automated Analysis of Cellular Signals from Large-
1086 Scale Calcium Imaging Data. Neuron 63, 747–760. https://doi.org/10.1016/j.neuron.2009.08.009
1087 Niell, C.M., Stryker, M.P., 2010. Modulation of visual responses by behavioral state in mouse visual
1088 cortex. Neuron 65, 472–479. https://doi.org/10.1016/j.neuron.2010.01.033
1089 Nomura, S., Bouhadana, M., Morel, C., Faure, P., Cauli, B., Lambolez, B., Hepp, R., 2014. Noradrenalin
1090 and dopamine receptors both control cAMP-PKA signaling throughout the cerebral cortex.
1091 Front. Cell. Neurosci. 8. https://doi.org/10.3389/fncel.2014.00247
1092 O'Toole, S.M., Oyibo, H.K., Keller, G.B., 2022. Prediction error neurons in mouse cortex are molecularly
1093 targetable cell types. https://doi.org/10.1101/2022.07.20.500837
1094 Pakan, J.M., Lowe, S.C., Dylda, E., Keemink, S.W., Currie, S.P., Coutts, C.A., Rochefort, N.L., 2016.
1095 Behavioral-state modulation of inhibition is context-dependent and cell type specific in mouse
1096 visual cortex. eLife 5, e14985. https://doi.org/10.7554/eLife.14985
1097 Polack, P.-O., Friedman, J., Golshani, P., 2013. Cellular mechanisms of brain-state-dependent gain
1098 modulation in visual cortex. Nat. Neurosci. 16, 1331–1339. https://doi.org/10.1038/nn.3464
1099 Rao, R.P., Ballard, D.H., 1999. Predictive coding in the visual cortex: a functional interpretation of some
1100 extra-classical receptive-field effects. Nat. Neurosci. 2, 79–87. https://doi.org/10.1038/4580
1101 Reimer, J., McGinley, M.J., Liu, Y., Rodenkirch, C., Wang, Q., McCormick, D.A., Tolias, A.S., 2016. Pupil
1102 fluctuations track rapid changes in adrenergic and cholinergic activity in cortex. Nat. Commun. 7,
1103 13289. https://doi.org/10.1038/ncomms13289
1104 Reynolds, J.N.J., Hyland, B.I., Wickens, J.R., 2001. A cellular mechanism of reward-related learning.
1105 Nature 413, 67–70. https://doi.org/10.1038/35092560
1106 Roelfsema, P.R., Holtmaat, A., 2018. Control of synaptic plasticity in deep cortical networks. Nat. Rev.
1107 Neurosci. 19, 166–180. https://doi.org/10.1038/nrn.2018.6

Sales, A.C., Friston, K.J., Jones, M.W., Pickering, A.E., Moran, R.J., 2019. Locus Coeruleus tracking of prediction errors optimises cognitive flexibility: An Active Inference model. PLOS Comput. Biol. 15, e1006267. https://doi.org/10.1371/journal.pcbi.1006267

Saravanan, V., Berman, G.J., Sober, S.J., 2020. Application of the hierarchical bootstrap to multi-level data in neuroscience. Neurons Behav. Data Anal. Theory 3, https://nbdt.scholasticahq.com/article/13927-application-of-the-hierarchical-bootstrap-to-multi-level-data-in-neuroscience.

Schneider, D.M., Sundararajan, J., Mooney, R., 2018. A cortical filter that learns to suppress the acoustic consequences of movement. Nature 561, 391–395. https://doi.org/10.1038/s41586-018-0520-5

Schultz, W., 2016. Dopamine reward prediction error coding. Dialogues Clin. Neurosci. 18, 23–32.

Schwarz, L.A., Miyamichi, K., Gao, X.J., Beier, K.T., Weissbourd, B., DeLoach, K.E., Ren, J., Ibanes, S., Malenka, R.C., Kremer, E.J., Luo, L., 2015. Viral-genetic tracing of the input–output organization of a central noradrenaline circuit. Nature 524, 88–92. https://doi.org/10.1038/nature14600

Seol, G.H., Ziburkus, J., Huang, S., Song, L., Kim, I.T., Takamiya, K., Huganir, R.L., Lee, H.-K., Kirkwood, A., 2007. Neuromodulators control the polarity of spike-timing-dependent synaptic plasticity. Neuron 55, 919–929. https://doi.org/10.1016/j.neuron.2007.08.013

Shepard, K.N., Liles, L.C., Weinshenker, D., Liu, R.C., 2015. Norepinephrine is necessary for experience-dependent plasticity in the developing mouse auditory cortex. J. Neurosci. Off. J. Soc. Neurosci. 35, 2432–2437. https://doi.org/10.1523/JNEUROSCI.0532-14.2015

Steinberg, E.E., Keiflin, R., Boivin, J.R., Witten, I.B., Deisseroth, K., Janak, P.H., 2013. A causal link between prediction errors, dopamine neurons and learning. Nat. Neurosci. 16, 966–973. https://doi.org/10.1038/nn.3413

Su, Z., Cohen, J.Y., 2022. Two types of locus coeruleus norepinephrine neurons drive reinforcement learning. https://doi.org/10.1101/2022.12.08.519670

Takeuchi, T., Duszkiewicz, A.J., Sonneborn, A., Spooner, P.A., Yamasaki, M., Watanabe, M., Smith, C.C., Fernández, G., Deisseroth, K., Greene, R.W., Morris, R.G.M., 2016. Locus coeruleus and dopaminergic consolidation of everyday memory. Nature 537, 357–362. https://doi.org/10.1038/nature19325

Vankov, A., Hervé-Minvielle, A., Sara, S.J., 1995. Response to novelty and its rapid habituation in locus coeruleus neurons of the freely exploring rat. Eur. J. Neurosci. 7, 1180–1187. https://doi.org/10.1111/j.1460-9568.1995.tb01108.x

Vasilevskaya, A., Widmer, F.C., Keller, G.B., Jordan, R., 2022. Locomotion-induced gain of visual responses cannot explain visuomotor mismatch responses in layer 2/3 of primary visual cortex. https://doi.org/10.1101/2022.02.11.479795

Vazey, E.M., Moorman, D.E., Aston-Jones, G., 2018. Phasic locus coeruleus activity regulates cortical encoding of salience information. Proc. Natl. Acad. Sci. 115, E9439–E9448. https://doi.org/10.1073/pnas.1803716115

Wagatsuma, A., Okuyama, T., Sun, C., Smith, L.M., Abe, K., Tonegawa, S., 2018. Locus coeruleus input to hippocampal CA3 drives single-trial learning of a novel context. Proc. Natl. Acad. Sci. 115, E310–E316. https://doi.org/10.1073/pnas.1714082115

Widmer, F.C., O'Toole, S.M., Keller, G.B., 2022. NMDA receptors in visual cortex are necessary for normal visuomotor integration and skill learning. eLife 11, e71476. https://doi.org/10.7554/eLife.71476

Yu, A.J., Dayan, P., 2005. Uncertainty, neuromodulation, and attention. Neuron 46, 681–692. https://doi.org/10.1016/j.neuron.2005.04.026

Zmarz, P., Keller, G.B., 2016. Mismatch Receptive Fields in Mouse Visual Cortex. Neuron 92, 766–772. https://doi.org/10.1016/j.neuron.2016.09.057